University of Central Florida

2024

Optical Seed Development For Yb-Fiber Laser

James G. Brutus
University of Central Florida

OPTICAL SEED DEVELOPMENT FOR YB-FIBER LASER

by

JAMES GODSON BRUTUS
B.S. University of Central Florida, 2022

A thesis submitted in partial fulfillment of the requirements
for the degree of Master of Science
in the College of Optics and Photonics
at the University of Central Florida
Orlando, Florida

Spring Term
2024

Major Professor: Martin Richardson

ABSTRACT

Master Oscillator Power Amplifiers (MOPA) are laser systems that utilize a seed and pump amplification system to boost the output power of high-quality lower power seeding signals. MOPAs can generate high gain while avoiding many of the nonlinearities that negatively affect resonance-based lasers that are known to feature higher internal intensities. Additionally, MOPAs provide an easy alternative to the construction of novel laser technologies for higher output power as they can be easily combined with existing laser sources to amplify their output power.

This thesis outlines the design of an ytterbium-doped fiber laser (YDFL), featuring a MOPA architecture. The YDFL is constructed to amplify a continuous wave single mode signal, at 1064nm, from 366mW to 16.4W while maintaining high spectral purity and beam quality. This laser is being developed with the intention to seed a subsequent MOPA YDFL for amplification to 1.5kW, for use in following thermal blooming experiments. As a result, the laser being developed in this work must have high spectral purity, centered near 1064nm, and a narrow linewidth, less than 0.25nm. Methods for limiting instabilities within the MOPA amplification stages are developed and the final seed laser emission quality is demonstrated in this work.

ACKNOWLEDGEMENTS

Stepping out of my comfort zone is something that I work on normalizing in my life. Discomfort can be accompanied by growth and accomplishment when graced by a guiding hand, and, throughout this work, I have been fortunate to have received a great deal of guidance from many of whom I would like to show my appreciation for.

I would like to thank Joshua Bryan for his contribution in laying down the framework for my M.S. thesis project and for his supervision throughout its development. I thank Dr. Martin Richardson and the Laser Plasma Laboratory (LPL) faculty for providing me with this opportunity to learn and test my knowledge in ways unparalleled to any other academic setting I have experienced. I would like to thank Zeus Gannon and Nick Vail who have mentored me in fiber laser development and have been there to answer the many questions that I have had. I thank Melissa Siver for introducing me to many fiber processing techniques needed for me to succeed in my project. I also thank the remaining members of LPL for their friendship, allowing me to feel welcome in this talented community. You all have made this experience worth all of my efforts, and more.

Lastly, I would like to thank my fiancé for her undying support and encouragement. You are my greatest blessing, and you are the reason why I strive to be better every day.

TABLE OF CONTENTS

LIST OF FIGURES

LIST OF TABLES

LIST OF ABBREVIATIONS

ASE   Amplified Spontaneous Emission

CW   Continuous Wave

DC   Double Clad

FBG   Fiber Bragg Grating

FWHM   Full Width at Half Maximum

HEL   High Energy Laser

IR   Infrared

LASER   Light Amplification by Stimulated Emission of Radiation

MASER   Microwave Amplification by Stimulated Emission of Radiation

MOPA   Master Oscillator Power Amplifier

NA   Numerical Aperture

Nd   Neodymium

OSA   Optical Spectrum Analyzer

P-I   Pump-Current

PM   Polarization Maintaining

TEC   Thermoelectric Controller

TEM   Transverse Electromagnetic

TIR   Total Internal Reflection

UV   Ultraviolet

VIS   Visible

Yb   Ytterbium

YDFL   Ytterbium Doped Fiber Laser

CHAPTER 1: INTRODUCTION

1.1 Motivation

Much of contemporary research in directed energy has focused on applications involving the ability to place high amounts of concentrated optical energy on targets up to several kilometers away in distance. Growing advocacy for directed energy from the Department of Defense has led to the contribution of billions of dollars for high energy laser (HEL) development for decades, furthering this area of research [1]. The objectives of these investments have been to develop systems that can eliminate range threats. Chosen for its general availability, versatility, and efficiency, lasers operating at 1064 nm have been integrated into a variety of defense-related high-power directed energy systems. The atmosphere is largely transparent to 1064 nm light and optical frequencies in the near-infrared range are capable of inflicting effective heating/ablation damage on interaction with a variety of materials. Despite this atmospheric transparency benefit, however, 1064 nm HELs for defense-related applications are not without their limitations.

An increasing inhibitor to high power near-infrared effectiveness in ranged atmospheric directed energy systems is a phenomenon known as thermal blooming. It is caused by absorption lines in the atmosphere by atmospheric gases. Of these, H_2O molecules, in the form of water vapor, is a primary contributor to the occurrence of thermal blooming near 1064 nm. These absorption lines contribute to the development of a self-induced refractive index gradient within a medium of propagation [2-4] that causes high power optical beams to diverge prematurely and lose their effectiveness proportional to the target distance.

The Laser Plasma Laboratory (LPL) within the College of Optics & Photonics and part of the Center for Directed Energy at the University of Central Florida is partnering with the Air Force

Institute of Technology to investigate thermal blooming in the atmosphere near 1064 nm by HEL systems using kW class single-mode YDFLs. Two 1.5 kW ytterbium (Yb) doped fiber laser systems are being developed, one spectrally fixed at 1064 nm and the other tunable between 1060-1090 nm. The outputs of each system will be coaxially combined so that the transient and interdependent beam-gradient effects can be investigated. This thesis details the design of a 16.4W YDFL, with a center wavelength and linewidth of 1064.8 nm and 0.21 nm respectively, that is constructed to seed the fixed wavelength kW YDFL.

1.2 Low Power Amplification Stage

The low power YDFL features a master oscillator power amplifier (MOPA) fiber laser architecture. It utilizes a 1064 nm continuous wave (CW) seeding diode with a narrow linewidth and single mode beam profile that is coupled from 5/125 µm (fiber core/cladding diameter) polarization maintaining (PM) fiber. The injected 366 mW signal from this device will be power scaled to 16.4 W. The power scaling will be accomplished in two separate 10/125 µm PM Yb-doped active-fiber amplification stages. The active fiber will be pumped by two 976 nm pump diodes, coupled from 105/125 µm multi-mode fiber, with peak powers at 10 W and 65 W, respectively. The desired beam output characteristics of the low power YDFL are a power output greater than 15 W, a center wavelength near 1064 nm, and a narrow linewidth, less than 0.25 nm. Additionally, noise from secondary radiative processes, such as amplified spontaneous emission (ASE) is undesirable. Therefore, a 40 dB signal-to-noise ratio is to be maintained. Instabilities such as free lasing and self-pulsing are also undesirable and are minimized. These instabilities are explained further in Chapter 2.

The following chapters provide a summary of the theory and history of fiber laser systems and their subcomponents. An analysis of the completed YDFL is performed. Included are relevant engineering considerations, sub-component and holistic system characterizations, and optimal operating specifications. The experimental procedures and fiber processing techniques utilized to optimize the system and obtain relevant characterizations are described. Characterizations on the final beam profile, spectral output, power scaling, conversion efficiency, beam polarization, and related temperature dependencies are provided.

CHAPTER 2: THEORETICAL BACKGROUND & CONSIDERATIONS

This section provides a general framework of already known physical sciences that were considered in the development of the low power YDFL. The architectures and subcomponent parts of fiber laser systems are contextually reviewed, prompting the investigation of fiber waveguides, amplification media, semiconductor laser diodes, and common fiber laser instabilities.

2.1 Fiber Lasers

Over 60 years ago, in 1960, T. Maiman expanded on Townes' concept of infrared and optical MASER (Microwave Amplification by Stimulated Emission of Radiation) and developed the first LASER (Light Amplification by Stimulated Emission of Radiation) [5, 6]. A laser is a device that emits energy in the form of highly coherent and monochromatic electromagnetic waves via stimulated emission in the ultraviolet-visible-infrared (UV-VIS-IR) wavelength range. The laser developed by Maiman utilized a solid rod of ruby that was pumped by a broadband flashlamp. Not long after the invention of the first laser, however, E. Snitzer published a paper on the demonstration of laser action from a barium crown glass fiber doped with neodymium ions (Nd^{3+}) in 1961 [7]. This laid the foundation for a new class of laser systems that utilized fiber waveguides.

Despite the original demonstration in 1961, fiber lasers did not rise in popularity until the advancement of fiber manufacturing processes and technologies in the late 1990s. The development of efficient semiconductor laser diode technologies and double-clad (DC) fiber pumping mechanisms, explained further in Chapter 2, have greatly increased the efficiency of fiber laser systems [8-10]. Since then, fiber lasers have been renowned for high diffraction-limited average power, which was possible due to the high optical intensities maintained by the waveguiding properties of optical fiber [11, 12]. Fiber laser systems are considered to be more

durable and compact than their free-space counterparts, leaving less room for misalignments to occur from external disturbances on the system. Additionally, they have high plug-in efficiency and are less costly to build than conventional laser devices [12]. These are factors which have led to fiber's adoption in many HEL applications.

2.1.1 High Power YDFLs & Advantages of MOPA Architecture

Ytterbium has become an increasingly leading rare-earth element used as a primary dopant in fiber based HELs [13]. It grew in popularity due to its broad gain bandwidth, spanning over 100 nm in the near-IR range (975-1180 nm) and the convenient overlap of its absorption band (900-980 nm) with widely available pump laser diode sources [12]. These qualities, combined with the low quantum defect experienced by laser diode pumping, high permissible levels of Yb-dopant concentrations in fiber, and efficient DC fiber pumping and thermal management techniques has led towards ytterbium's adoption for countless high power laser projects. In LPL, YDFLs with multi-kW average output powers and single mode operation have been demonstrated [14].

In the construction of high-power YDFLs, standard laser resonator architectures, such as Fabry-Perot architectures, shown in Figure 1, can prove to be problematic. The broad gain bandwidth of Yb-doped fiber, without fiber Bragg gratings (FBGs), can lead to the generation of linewidths on the order of 10nm [15, 16], which is too broad to meet the intended purpose of our narrow linewidth system. The intracavity field intensities can be significantly higher than those emitted in optical resonators. The high intensities stimulate disruptive nonlinear processes such as the Kerr effect, stimulated Raman scattering, and stimulated Brillouin scattering leading to a tradeoff between beam quality and power [17, 18]. Additionally, the high intracavity intensities present in optical resonators result in increased thermal activity within the laser cavity. Preventative measures

against these instabilities are difficult to implement due to the closed resonator system in which amplification takes place. Characteristics of a high-quality signal, such as narrow linewidth, are often decoupled from high power generation in optical resonators because of these effects.
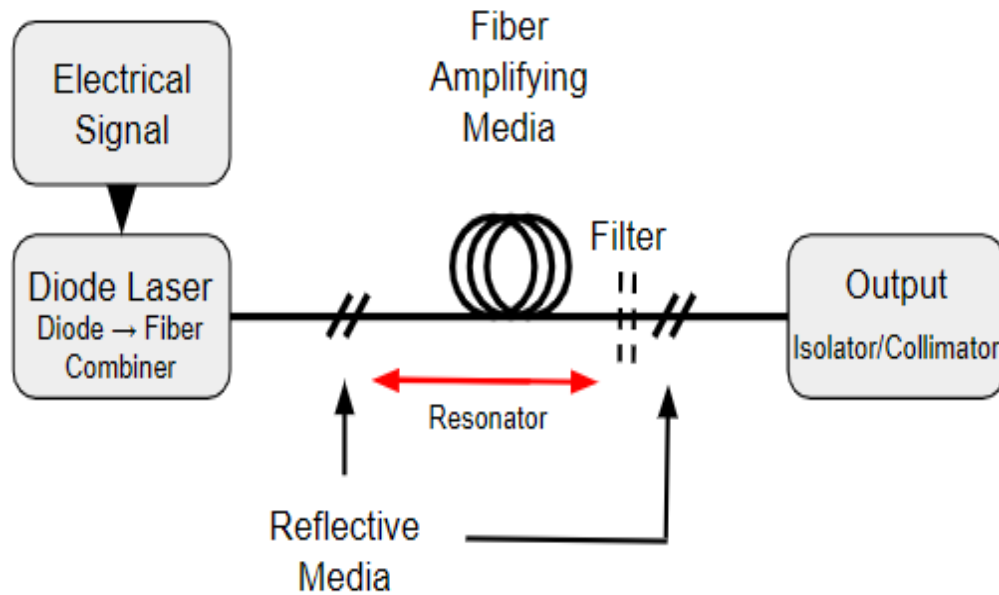
Figure 1: Architecture for a Fabry-Perot fiber laser cavity. This architecture utilizes the standard resonator concept to promote stimulated emission.

To work around these limitations, a particular fiber laser architecture has been established that utilizes a technique known as injection locking. A low power, high quality, optical master oscillator is fine-tuned to achieve desired spectral and spatial profiles and is injected into an optical gain media. Optical pumps then saturate the optical gain media, raising electrons to their excited states, allowing the injected signal to subsequently induce stimulated emission at the signal wavelength [19]. This setup is known as a MOPA laser architecture, depicted in Figure 2.

In a MOPA, the signal is amplified unidirectionally, resulting in a more linear relationship between internal intensities and the emitted output power. As a result, MOPAs are less susceptible to the degenerative processes that affect signal development in high power optical resonators. This provides more room for power scaling while minimizing the disruptive effects caused by intensity dependent nonlinearities.

The separation between the signal development and amplification stages allows for the implementation of beam quality maintenance devices, like isolators and cladding light strippers, at various stages of the signal's development in the MOPA. It also allows for the introduction of advanced thermal management techniques since the heat produced from cladding pumped gain media can be spread over longer lengths of fiber. This provides flexibility for the minimization of instabilities, such as ASE, between intermediate amplification levels [20], while retaining the original signal quality. The output can also be continually cascaded into further amplification stages.
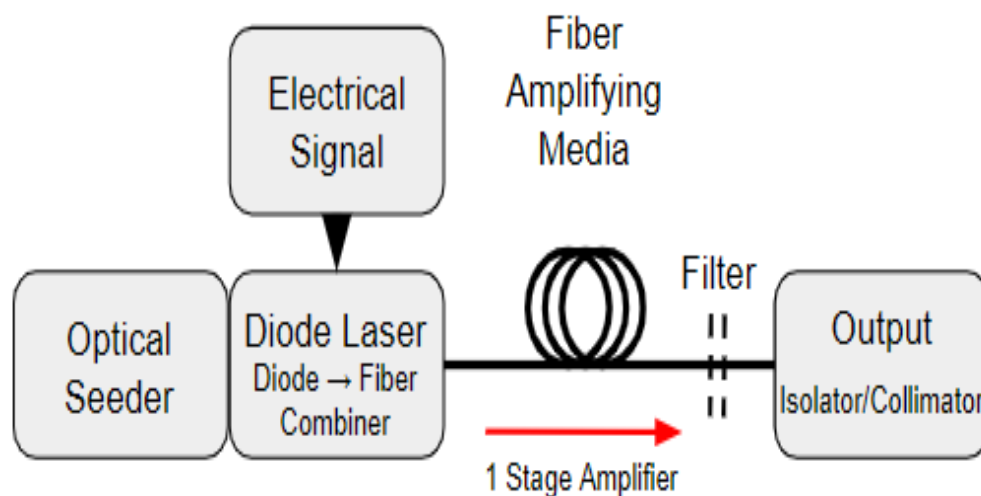
Figure 2: Architecture for a MOPA laser. This architecture utilizes a seed signal that is scaled by optically pumped fiber amplifying media.

2.2 Optical Fiber Amplification & Gain Media

The rare earth element utilized as the laser active dopant in this system is ytterbium. It is present as the trivalent ion, Yb^{3+} in the host 10/125 µm silica-based fiber, SiO_2. This section provides information on the use of ytterbium as the doping agent for the spectrally fixed fiber laser. Details regarding ytterbium's electron energy levels, absorption/emission spectra, and the amplification dynamics are provided.

2.2.1 Ytterbium Energy Levels & Absorption/Emission Spectra

Pumping and amplification occurs from transitions between the various sublevels of the Yb electron excited and ground state Stark level manifolds. The Yb^{3+} ion features the $^2F_{5/2}$ and $^2F_{7/2}$ energy levels between which broad absorption and emission bands exist, Figure 3, due to the inhomogeneous media, SiO_2, the Yb is present in. There are strong absorption bands near 915 nm

and 976 nm and strong emission bands between 980-1150 nm. The broad gain bandwidth allows for the development of Yb-based laser systems spectrally tunable over 90 nm [21]. Additionally, due to the proximity between the ground state and pump state energy levels, there is an observed quasi-three-level behavior that exists in Yb-based gain media. This behavior is exhibited in the reabsorption of the emission laser wavelength, resulting in the overlap in the absorption/emission spectra.
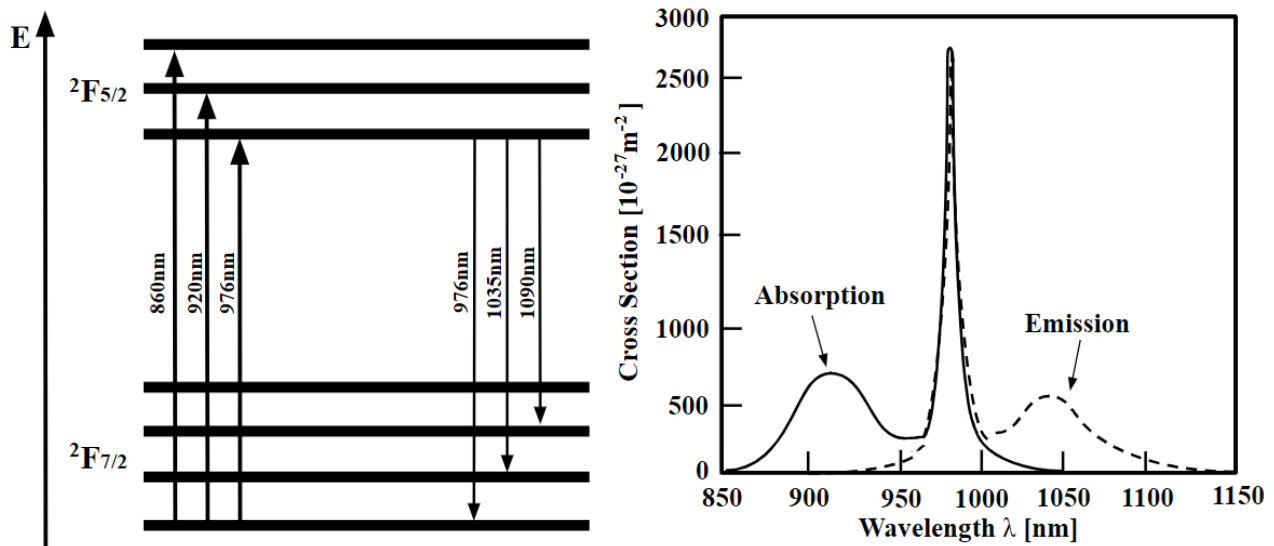
Figure 3: [Left] Ytterbium electron energy levels and sublevels. The $^2F_{5/2}$ lines denote the excited state sublevels, and the $^2F_{7/2}$ lines denote the ground state sublevels [22]. [Right] Typical absorption/emission spectra of Yb^{3+} doped silica fiber, SiO_2 [23-27].

Transitions between energy levels can occur from either radiative or nonradiative processes. Spontaneous emission and stimulated emission are the processes by which radiative decay to lower energy levels occur, whereas the non-radiative processes include intra-material interactions that release energy largely in the form of thermal energy. This difference in energy, called the quantum defect, is represented by q in the following:

$$q = h\nu_{pump} - h\nu_{laser}$$

Where q represents the quantum defect (in J or eV), Planck's constant is given by h = 6.626*10^-34^Js = 4.14*10^-15^eVs where 1eV = 1.602*10^-19^J. Additionally, ν_{pump} and ν_{laser} are the frequencies (in Hz) of electromagnetic radiation for the pump and signal. The quantum defect experienced by a 976 nm pumped Yb^{3+} for 1064nm lasing is 99.3 meV. This is less than the 349 meV defect experienced by 808 nm pumped neodymium (Nd^{3+}) 1064 nm lasing. For this reason, less heat generation and greater pumping efficiency is observed in Yb-doped lasers operating at 1064 nm [23].

Stimulated emission is the only process desired for laser amplification as it contributes to the generation of largely monochromatic, coherent light. For efficient laser action to be achieved, radiative and non-radiative processes other than stimulated emission need to be limited. The theoretical considerations needed for the optimization of these processes for efficient laser action is provided in the next section.

2.2.2 Ytterbium Fiber Amplification Dynamics

The following simplified set of carrier rate equations can be derived by statistically representing the ground and excited energy levels of a Yb-doped silica fiber amplifier as [27-29]:

$$\frac{dN_2}{dt} = (R_{12} + W_{12})N_1 - (R_{21} + W_{21} + A_{21})N_2$$

$$\frac{dN_1}{dt} = (R_{21} + W_{21} + A_{21})N_2 - (R_{12} + W_{12})N_1$$

Where A_{ij} represents spontaneous decay rates, W_{ij} is the stimulated emission rates, R_{ij} the pumping rates all measured in Hz. N_i & N_j are the population densities (in m^-3^), with i and j indicating the

relevant energy levels. A more dynamic statistical representation of the quasi-three-level behavior is provided by T. Taira for Yb gain media [30]. In these simplified equations, ASE, is assumed to have a negligible impact on the transition rates. Under steady-state CW conditions, $N_1 + N_2 = 1$, the transitions rates can be derived as:

$$R_{12} = \sigma_{ap} \frac{I_p}{h v_p} \qquad R_{21} = \sigma_{ep} \frac{I_p}{h v_p}$$

$$W_{12} = \sigma_{sp} \frac{I_s}{h v_s} \qquad W_{21} = \sigma_{sp} \frac{I_s}{h v_s}$$

Where σ_{ap} and σ_{ep} are the absorption/emission cross-sections for the pump (in m^2), σ_{as} and σ_{es} are the absorption/emission cross-sections for the signal (in m^2), I_p and I_s are the intensities (in W/m^2), and v_p and v_s are the frequencies of the pump and signal respectively. The pump saturation power, P_s (in W), which is the power at which increases in pump power no longer contributes to an increase in the emission power, can be expressed as [23]:

$$P_s = \frac{h v_p A}{(\sigma_{ep} + \sigma_{ap}) \tau \phi_p}$$

Where A is the cross-sectional area of the gain medium (in m^2) and ϕ_p is the pumping quantum efficiency, which is a measure of how efficiently pump power is converted into laser signal power. This is separate from the quantum defect, which is the difference in energy between a pump and signal photon. $\phi_p = 0.92$ for a seeding and pump wavelength of 1064 nm and 976 nm, respectively [23]. τ denotes the upper-state lifetime (in s) and σ_{ap} and σ_{ep} are the absorption and emission cross sections at the pump wavelength, measured in units per area (in m^{-2}). The unsaturated gain, per unit length, L (in m), is G_0, and the single pass gain, expressed in dB, equal to $10\log(P_{Out}/P_{In})$, is provided as $g(\lambda)$.

$$G_0 = g_0 L = \frac{P_a}{P_s} - N\sigma_{al}L$$

$$g(\lambda) = 10log(G_0)$$

The unsaturated gain is a characteristic of laser operation at power levels beneath that of maximum output power. When a gain media is saturated, the population inversion reaches a level that cannot support any additional stimulated emission. This is because all of the available ions for stimulated emission are already in the excited energy states. In unsaturated gain laser option, the relationship between input pump power and output signal power is approximately linear. The relationship becomes nonlinear when operating in the saturated regime.

Modern Yb^{3+} fiber amplifiers achieve power conversion efficiencies greater than 75% [12, 27] with amplifier gain between 10-30 dB/m, from Ter-Mikirtychev [23]. The calculated gain for Yb-fiber at various signal and pump wavelengths is provided in Figure 4.
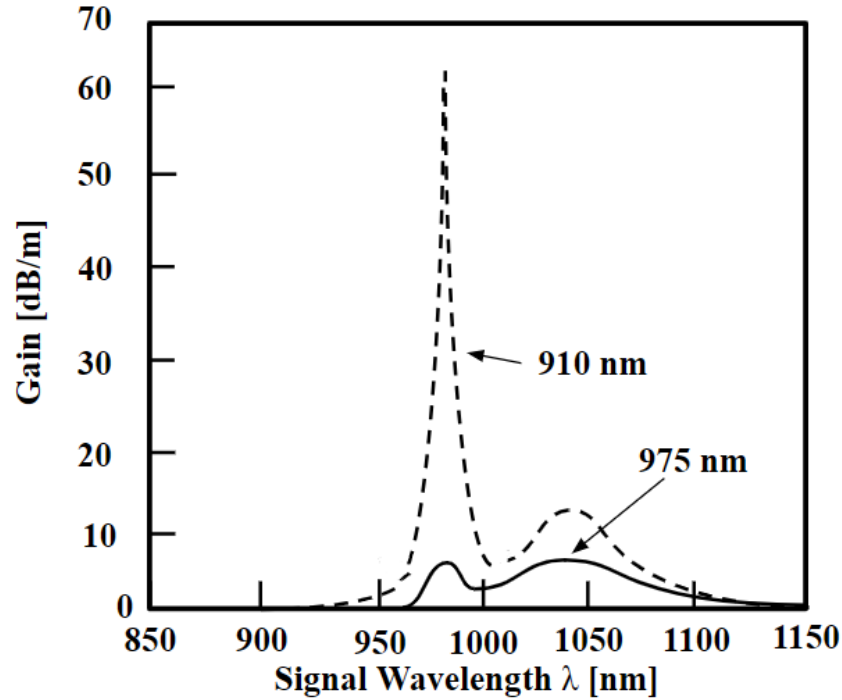
Figure 4: Calculated gain spectra for a Yb-doped germanosilicate fiber (1000 ppm by weight) with 910 nm and 975 nm pumps [27].

The 1064 nm Yb-doped fiber laser transition has a relatively long upper state lifetime, although it varies strongly with different hosts materials, dopant concentration, and temperature [31]. These variables can contribute to increased or decreased quenching, or suppression, of fluorescence in the gain media. Yb doped glass fibers feature an upper state lifetime on the order of 1 ms at room temperature [31, 32] whereas Nd doped glass fibers feature shorter lifetimes in the μs regime [33, 34]. This comparison persists for Yb and Nd doped in yttrium aluminum garnet (YAG). Here, Yb:YAG features a longer upper state lifetime at 950 μs and Nd:YAG has a shorter lifetime at 230 μs [23, 35-37]. The longer upper state lifetimes for Yb contributes to lower transition cross-sections for Yb doped gain media. This is beneficial for pulsed laser operation; however, it can prove to be detrimental for CW laser operation.

Yb:YAG features relatively sharp absorption lines as the ions are imbedded within a homogeneous crystal lattice. In Yb-doped fibers, the ions are loosely embedded in and inhomogeneous glass matrix. This results in broader absorption bands than their crystal host counterpart, making them more versatile with respect to potential pumping candidates. Decreased selectivity of transition wavelengths, however, can lead to increased ASE, and furthermore, a decrease in laser performance and signal amplification. Additionally, one must also consider temperature-related effects. One of the most common effects seen in laser gain media is thermal broadening. At higher temperatures, the distribution of molecular velocities relative to the observer broadens which results in Doppler-broadened spectral lines, that blurs the fine details in high spectral quality signals.

2.2.3 Ytterbium Fiber Modeling

To ensure efficient absorption and amplification at the signal wavelength, the appropriate lengths and concentration of Yb-doped fiber must be utilized. The fiber used in the construction of the Yb-doped MOPA fiber laser is the polarization maintaining large mode area Yb-doped double clad fiber with a 10/125 µm core/cladding fiber diameter (PLMA-YDF-10/125-HI-8) from Coherent, Inc. The dopant concentration of the Coherent, Inc. fiber is proprietary, however, the cladding absorption near 975 nm is provided to be 6 dB/m.

Using a credible third-party modeling software, RP Fiber Power (Version 7; R. Paschotta, 2020) [38], the necessary lengths of fiber needed for efficient pump absorption was calculated. The software assumes constant dopant concentration and perfect pump power coupling into the core then utilizes the known rate equations and absorption/emission cross-sections of ytterbium to estimate pump absorption and signal gain.

First, the expected concentration of Yb^{3+} ions present in the Coherent fiber was approximated using a fiber amplifier small signal gain approximation [38, 39]. In the approximation, a negligible signal and small pump power is modeled through the fiber featuring an active core diameter of 10 µm. The concentration of ions needed to approximate pump absorption to 6 dB/m is then acquired to be $N_{Yb} \approx 85*10^{24}$ cm^{-3}. Once the estimated dopant concentration was found, the experimentally measured amplifier injection powers, (see Chapter 4) for the signal and pump were used to estimate fiber lengths for efficient pump power conversion. 348 mW seed and 8.18 W pump power were modeled for amplifier 1 and 4.68 W signal and 56.1 W pump power were modeled for amplifier 2. The results from the modeling software are provided in Figure 5.
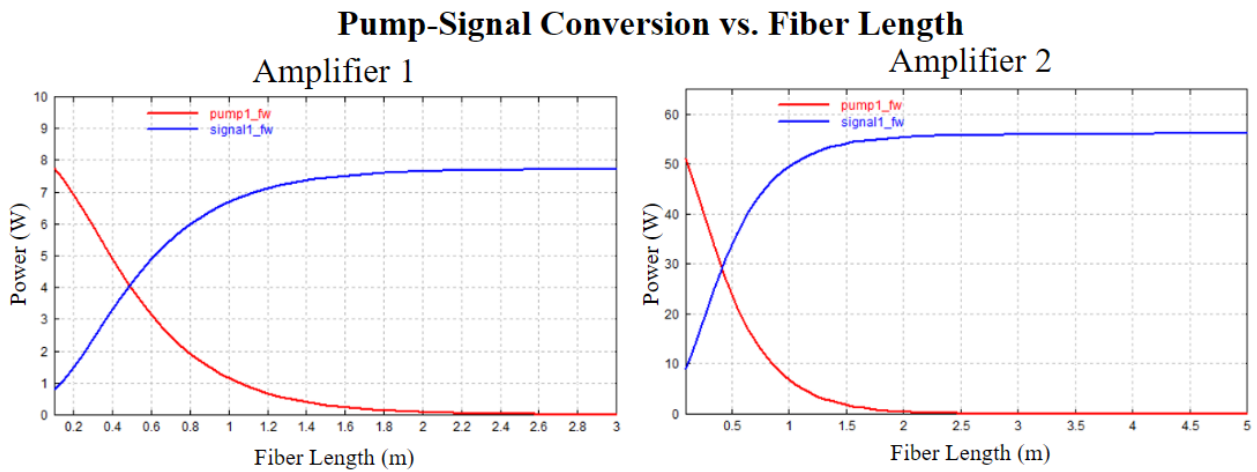
Figure 5: RP Fiber Power fiber length approximations for efficient pump power conversion [38].

Referencing the results from the modeling software, an increase in pump power conversion is observed as fiber length increases. There is sufficient pump absorption, ≳ 95% total pump power, at fiber lengths greater than 1.5 m and 2.5 m for the first and second amplification stages. Due to variations between the assumptions of the modeling software and the actual experimental parameters, such as perfect pump power coupling and negligible losses at the fiber splice points, fiber lengths greater than 1.5 m and 2.5 m will be utilized. Experimentally, the lengths of

amplifying fiber chosen are 2.5 m and 4.5 m. Ultimately, in Chapter 4, they are tested for pump power absorption and ASE generation to determine if they meet the requirements of the system.

2.3 Semiconductor Laser Diodes

As briefly introduced in the history of fiber lasers, it was the growing efficiency and availability of laser diodes sources that contributed towards the practicality and advancement of fiber laser technology. The ability to continuously produce high optical power at a variety of specific wavelengths was essential for efficiently pumping the narrow absorption windows of rare-earth doped laser gain media. This section summarizes their operation and role within fiber laser systems.

In semiconductor laser devices, electrons are excited from stable low energy states to high energy states via the application of an electric potential. This process is called excitation and when it occurs an electron 'moves' from the valence band to the conduction band of a material leaving behind a 'hole' in its stead. The high energy states are unstable; therefore, excited electrons return to their previous low energy states in a process known as relaxation. The recombination of the electron and the hole in the relaxation process can be either radiative or nonradiative. It is radiative recombination that results in the emission of optical energy, luminescence, whereas non-radiative recombination contributes to non-optical forms of energy transfer, such as thermal energy.

The energy required to induce an electron transition to the conduction band is called the bandgap energy, E_g. This energy is the difference between the valence and conduction band. This energy difference can be met by a single photon of wavelength $\lambda_g = hc/E_g$ or by external application of an electric potential. Excited electrons, upon interaction with an incident photon with sufficient energy will emit two coherent photons of equal energy and phase. The so-called quasi-Fermi levels

16

are given by E$_{fc}$ and E$_{fv}$. These are the levels used to describe the distribution of charge carriers in a non-thermal equilibrium state. See Figure 6 for a graphical representation of the semiconductor bandgap structure.
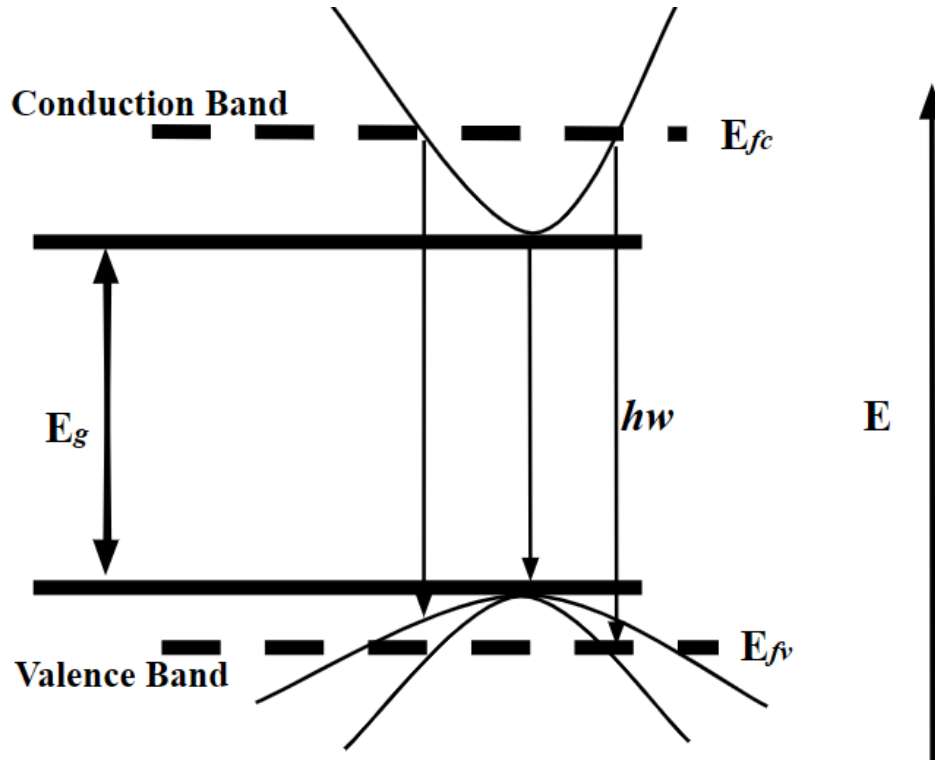
Figure 6: Semiconductor band structure depicting direct bandgap transitions between the conduction and valence bands [40]. Indirect bandgap transitions may include phonon-coupling.

The electron and hole concentrations, developed from the injection of electrical current in semiconductor devices are given by n and p (in m^{-3}) respectively:

$$n = N_c exp\left(-\frac{E_c - E_{FC}}{k_B T}\right) \qquad\qquad N_c = 2\left(\frac{2\pi m_e * k_B T}{h^2}\right)^{3/2}$$

$$p = N_v exp\left(-\frac{E_{Fv} - E_v}{k_B T}\right) \qquad\qquad N_v = 2\left(\frac{2\pi m_h * k_B T}{h^2}\right)^{3/2}$$

Where E_c and E_v are the respective conduction and valence band energies (in J or eV), N_c and N_c are the effective density of states (in m^{-3}) [41]. The Boltzmann constant is provided by $k_B = 1.38*10^{-23}$ J/K $= 8.62*10^{-5}$ eV/K. T is temperature (in K) and m_e and m_h are the effective masses of electrons and holes (in kg).

We see that when the operating temperature of a semiconductor increases, there is a corresponding increase in the width of the distribution of carrier energies leading to spectral broadening. Additionally, the center wavelength of laser diodes increases with increasing operating temperature. This quality is measured as the wavelength temperature coefficient, and it is the result of temperature dependent bandgap variances and the thermal expansion/contraction of the semiconductor active media which can affect the optical properties of the emitted wavelength. These effects are characterized for the selected laser diodes used in the construction of the YDFL. The thermal effects are not ideal, and an investigation of several diode cooling mechanisms will be performed in Chapter 3. Cooling methods will be employed to mitigate the degree of thermal broadening and wavelength shift so that the system operates optimally.

Assuming an equal concentration of electron and hole concentration, the following rate equation can be formulated, from Numai [41]:

$$\frac{dn}{dt} = \frac{J}{ed} - G(n)S - \frac{n}{\tau_n} \qquad\qquad \frac{1}{\tau_n} = \frac{1}{\tau_r} + \frac{1}{\tau_{nr}}$$

Where S is the photon density (in m^{-3}), G(n) is the stimulated emission amplification rate (in s^{-1}), J is the injected current density (in Am^{-2}), the charge of an electron is given by e $= 1.602*10^{-19}$ C, d is the active layer thickness (in m), n is the carrier concentration (in m^{-3}), and τ_n is the carrier lifetime given by the radiative, τ_r, and nonradiative τ_{nr}, recombination lifetimes expressed in seconds. Below threshold, photon density is nil, so S $= 0$, and in steady state operation there is no

change in carrier concentration over time, so dn/dt = 0. This allows us to represent the carrier concentration, n, and furthermore, the threshold current density, J_{th}, as:

$$n = \frac{J}{ed}\tau_n \qquad\qquad\qquad J_{th} = \frac{ed}{\tau_n}n_{th}$$

Each semiconductor laser diode has a characteristic current threshold condition that is required before lasing is achieved. The threshold current is the point at which enough current is applied to induce population inversion, where the concentration of carriers in the excited state surpasses that of the ground state in the active medium. The threshold current varies with the respective material, temperature, and geometric properties of the diode.

When the current supplied through a semiconductor increases beyond the threshold condition, the ratio of optical power output with respect to the injected current is characterized by the slope efficiency, S_{dj} [41]. The "dj" stands for differential junction, associated with the differential behavior of the diode junction. This efficiency is often depicted in power-current (P-I) curves for individual diodes, showcased in Figure 7. This value is utilized to characterize the general effectiveness of laser diodes and it will be experimentally obtained for the semiconductor laser diodes chosen in the development of our laser system. We will observe variations in the efficiency due to changes in temperature.

$$S_{dj} = \frac{\Delta P_j}{\Delta I}$$
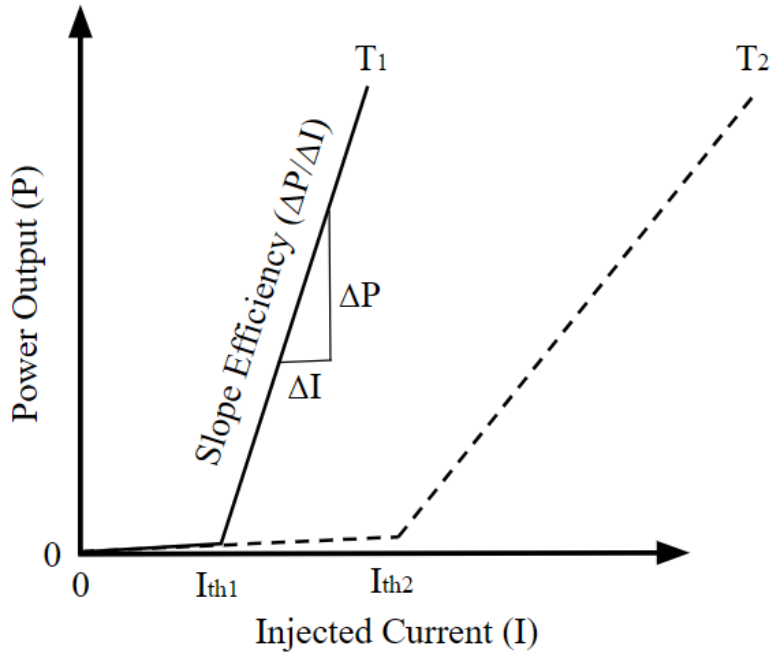
Figure 7: General laser diode P-I curve featuring slope efficiency and temperature dependence, where $T_1 < T_2$ [41].

The Yb fiber laser system that is the subject of this thesis features two semiconductor devices that are utilized as the pump sources for the gain amplifier. Wavelength matching of the gain media absorption bands is a primary limiting factor for pumping components. Conveniently, many commercially available high-efficiency diodes, are based on direct band gap gallium arsenide (GaAs), $E_g = 1.441eV$, or indium phosphide (InP) materials, $E_g = 1.35eV$, that operate in a wavelength range (940-980 nm). This complements the absorption band of ytterbium ions. Commercially available semiconductor devices made from these materials tend to be stable in their emission bandwidths and power-current curves. Additionally, they can be purchased prepackaged with fiber couplers for straightforward integration into fiber systems. The semiconductor laser diodes that have been chosen to pump the YDFL feature stable emissions at 976 nm that help to optimize the amplification process. The seed laser diode features a linear polarization state that will be maintained through the use of PM fiber throughout the YDFL's construction.

2.4 Laser Instabilities

As a fiber laser is developed, instabilities may arise that can affect the laser action of the system. The instabilities can be induced by a variety of internal and external mechanisms that result in fluctuations in the quality of the laser emission. Some common laser instabilities include thermal broadening of spectral lines, linear and nonlinear scattering processes, and external perturbations [42, 43]. In the MOPA being developed here, the laser instabilities that are the most prevalent and limiting are ASE and internal parasitic lasing [44]. These instabilities can determine the maximum gain that can be achieved in fiber amplifiers [45, 46]. This section will provide a brief context on the cause of these instabilities, their impact, and the methods implemented in design to minimize them.

2.4.1 Amplified Spontaneous Emission

The fluorescence from spontaneous emission that occurs in optical gain materials can be amplified, given the right conditions. Traditionally, spontaneous emission is known to emit optical radiation omnidirectionally, however, when confined within a highly saturated waveguiding media such as doped active fiber, the spontaneous emission propagating along its length can compete with the signal for gain. The spontaneous emissions can undergo amplification similar to that of stimulated emission in a media with high gain [45, 47].

Since the emission gain linewidth for Yb-doped fiber pumped at 976 nm extends from 1030-1100 nm, we can expect fluorescence emissions anywhere in this wavelength range since spontaneous emission is not driven by any particular signal and is susceptible to a range of Stokes' shifting processes. As a result, ASE is seen as an undesirable effect within MOPA laser emissions. It is the dominant noise term in fiber amplifiers, blurring the emission linewidth with unwanted frequencies

that lie outside the primary signal linewidth. It also suppresses signal amplification by exhausting excited energy state populations. Additionally, as ASE propagates through a laser system, the noise can become continually amplified in latter amplification stages, increasing the level of noise surrounding the primary signal and decreasing the apparent signal-to-noise ratio. This is why it is crucial that ASE is minimized at every intermediate stage within the fiber laser system.

ASE cannot be fully eliminated internally within high gain media because it is a result of the same optical processes needed for stimulated emission,. As a result, to ensure that the subsequent amplification of ASE remains manageable, methods involving the careful balancing of fiber length and pump intensity to maximize signal amplification and minimize ASE amplification, have been developed [48, 49].

Increasing fiber length or dopant concentration allows for more pump absorption and transition into the signal frequency emission. However, extending past the fiber length and dopant concentration threshold at which the maximum pump absorption is met, allows for the signal to be reabsorbed and emitted in the form of spontaneous emission. The effects of ASE may also be minimized by strengthening the signal power relative to that of the pump. In the construction of the MOPA YDF laser, amplified fiber lengths and signal powers incident at each amplification stage will be set such that the ASE amplitude is at a 40-50 dB difference from the signal peak.

2.4.2 Parasitic Lasing & Self Pulsing

Parasitic lasing is a phenomenon in which unintentional laser action takes place for an enclosed beam path "by virtue of some internal feedback", from Svelto [45]. In fiber optics, this unintentional laser action can be triggered by reflections on the end-facet of a fiber, in most cases caused by non-optimal cleave angles that result in total internal reflection (TIR) of meridional rays

with complimentary incident angles with the fiber end. These reflections contribute towards the development of a quasi-resonator cavity within an amplification fiber that exists for a fraction of the light propagating through the fiber. This leads to the generation of optical amplification modes, separate from the primary, that can induce laser action at undesirable frequencies, hence the term, parasitic lasing.

Observing laser emissions suffering from parasitic lasing on a spectrum analyzer may reveal spikes of optical power separate from the primary signal [50]. This contrasts with the broader gain windows observed in the spectral output of ASE. Parasitic lasing is detrimental to fiber laser systems for the same reason ASE is, as they both contribute to the generation of undesirable frequencies in a laser's emission which subtract the gain availability from the primary signal intended to undergo amplification.

Internal resonances may also contribute towards the development of self-pulsing in a fiber laser system. Parasitic lasing and self-pulsing is most prevalent when there are a large quantity of excited ions that are left unstimulated by the signal, and therefore available for laser action in separate channels [50]. Self-pulsing is a phenomenon in which short pulses with high peak power are generated through resonant laser instabilities. They can be caused by a multitude of internal laser instabilities such as mode-competition and gain fluctuation which become more prevalent in systems where random resonance is induced. The powers generated by self-pulsing can be catastrophic for high peak power pulsed laser systems as well as CW systems [50, 51], as the peak powers generated from self-pulsing can exceed the damage threshold of the passive fiber components or the active fibers themselves.

In a MOPA fiber laser, amplification is obtained without inducing an effect where the signal passes through the amplifying media multiple times. In their construction, it is important that the amplified fiber ends are angularly cleaved, following a technique outlined later in Section 2.5.1, to avoid TIR when sampling the laser emission. This helps to avoid the creation of internal resonances that may lead to internal instabilities such as parasitic lasing and self-pulsing that are detrimental to the concept of a MOPA fiber laser system. Isolators may also be used to remove backwards propagating light.

2.5 Fiber Waveguides

The general design of an optical fiber is centered around their waveguiding capability which is the ability to channel optical energy through defined spaces and directions. Optical fibers may come prepared with additional characteristics that can manipulate the polarization, modality, and power of the traversing optical signal. This section summarizes these capabilities and outlines the structures needed to maintain them.

2.5.1 Principles of Fiber Waveguides

The structure for a standard step-index fiber waveguide includes multiple layers starting with a core at the very center with a surrounding cladding, Figure 8. Additionally, optical fibers may come prepared with a buffer, made of a polymer material. The polymer may feature a lower index of refraction than the cladding to enable the cladding to act as a waveguide. The addition of a polymer may also function as a guard, protecting the inner cladding from external elements. A fiber jacketing material may also be added to further strengthen and protect the fiber from the stresses it may be exposed to in processing and use.

The index of refraction of the core, n_{core}, is engineered to be higher than that of the cladding, $n_{cladding}$, to take advantage of TIR. This is the phenomenon that allows fibers to act as waveguides for particular wavelengths, and it can be verified using Snell's Law. If ($n_{core} = n_1$) > ($n_{cladding} = n_2$), θ_2 cannot exceed a critical angle, θ_c, shown in Figure 8 and given by:

$$n_1 sin(\theta_1) = n_2 sin(\theta_2)$$

$$\theta_c = arcsin(\frac{n_2}{n_1})$$
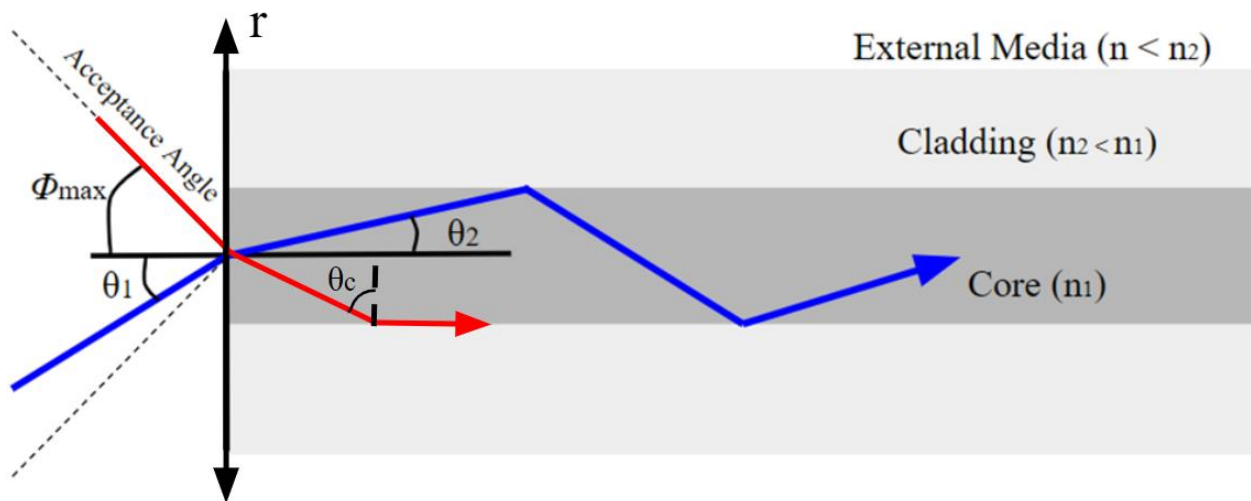
Figure 8: The structure of a fiber waveguide. The buffer and jacketing are not shown [52].

The numerical aperture (NA) is a measurement of the maximum acceptance angle of a fiber and it is a characteristic commonly associated to optical fibers. Rays entering the fiber at Φ_{max} will be incident on the core-cladding interface at the critical angle, which is the angular threshold for which TIR can persist, as shown in Figure 8. The NA is given by:

$$NA = \sqrt{n_1^2 - n_2^2} = nsin(\phi_{max})$$

When outcoupling fiber light into free space, the fiber end must be prepared such that the cleave angle minimizes internal reflections at the fiber end, Figure 9. This is important as MOPA fiber lasers are highly susceptible to damage from backwards propagating light since they can contribute toward the development of free-lasing instabilities. To minimize internal reflection, the cleave angle, θ, must satisfy the following inequality:

$$cos^{-1}\left(\frac{n_2}{n_1}\right) \; < \; \theta \; < \; sin^{-1}\left(\frac{1}{n_1}\right) - cos^{-1}\left(\frac{n_2}{n_1}\right)$$
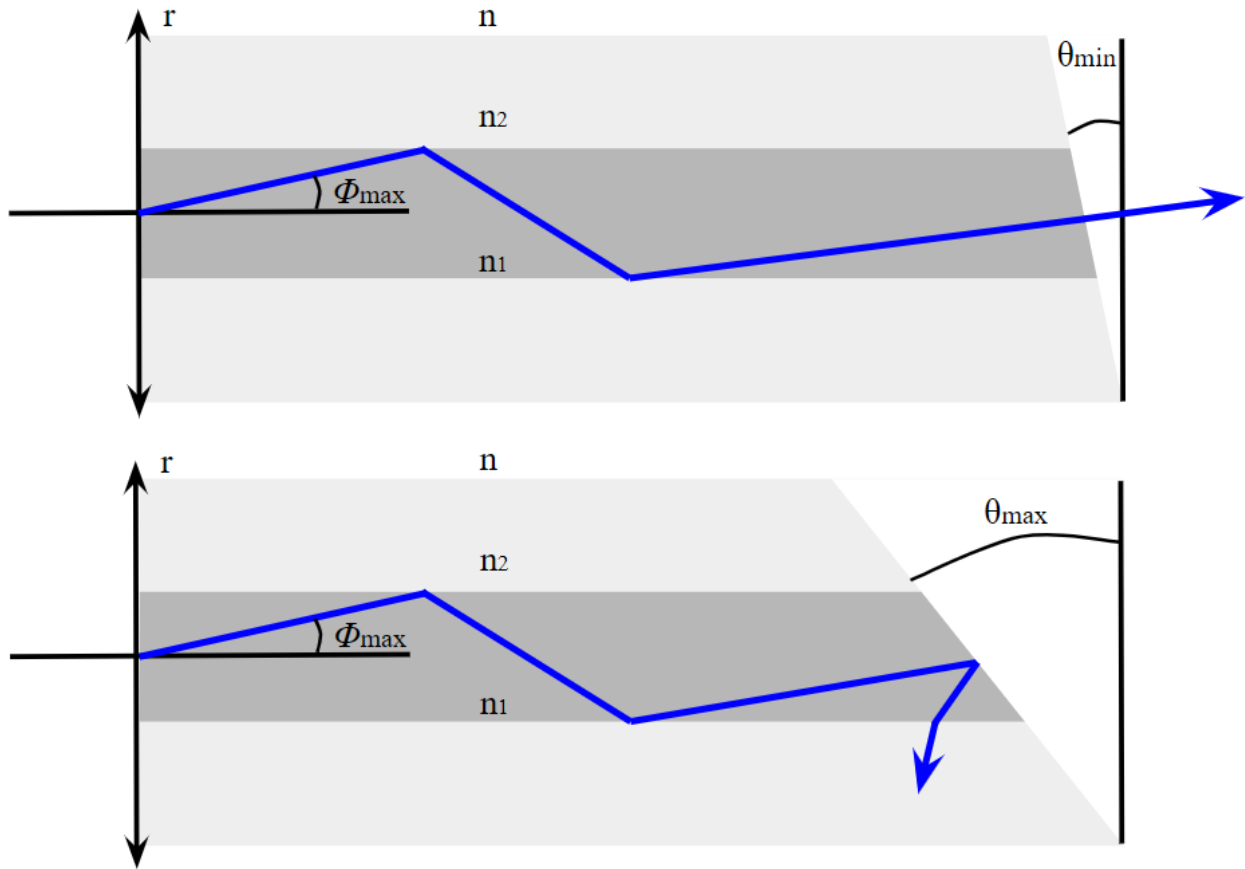
Figure 9: In (a) the extreme meridional ray is reflected on itself. In (b) the extreme meridional ray is totally internally reflected at the end surface. If the angle θ is made larger than this value, more of the useful rays will be totally reflected and thereby lost for purposes of amplification, from Tynes, A. R. [53].

Optical fibers can be manufactured to support either single or multimode operation. This is dependent on the NA, wavelength and radius of the fiber core, a. A fiber mode refers to the various spatial configurations light can populate within a fiber. Figure 10 showcases various fiber propagation modes and the conceptual difference between single-mode and multimode fibers. The number of guided modes can be determined by the V number. Single-mode operation is obtained for V $\lessapprox$ 2.405 [23]. Hence, we expect lower diameter cores in single-mode fibers. The fiber that will be utilized to carry the primary signal in the construction of the Yb-doped MOPA fiber laser is a 10/125 µm fiber with a core NA of 0.075. To carry a signal of 1064 nm, the V number can be calculated as such:

$$V = \frac{2\pi a}{\lambda} NA = \frac{2\pi \left(\frac{10 * 10^{-6} m}{2}\right)}{1064 * 10^{-9} m} (0.075) = 2.214 \lessapprox 2.405$$
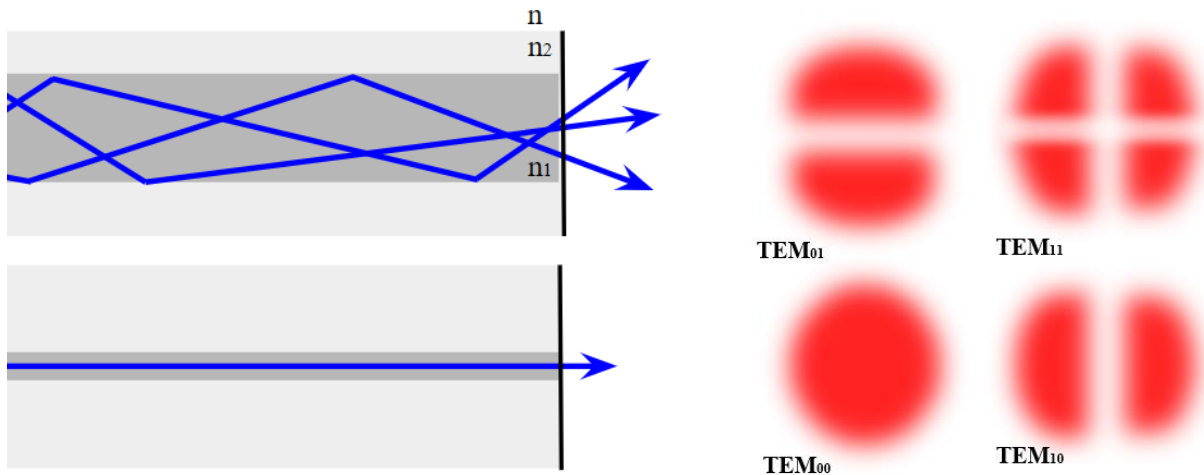
Figure 10: [Left] Multimode fiber, top, represented with various optical wave spatial configurations and single-mode fiber, bottom. [Right] The projection of a single and multi-mode emissions in the transverse plane. Single-mode fiber emissions follow the fundamental transverse electromagnetic (TEM$_{00}$) gaussian intensity profile.

This verifies that the condition for single mode operation is met for the signal carrying fibers. The pump, however, will be experiencing multimode operation as it traverses a larger radial cross section within the cladding of the fiber. The effective radius of the inner cladding is 62.5 µm and the first cladding NA is 0.46. This results in a V number of 185.08, satisfying the multi-mode condition. For multi-mode fibers, the number of modes can be approximately provided as $M = 4V^2/\pi^2$ [23], which is 13883 modes for pump light traversing the signal fiber. A diagram of mode effective index of refraction as a function of V number that depicts available mode profiles can be found in this resource, [54].

The fiber used to carry the signal features a DC PM structure, Figure 11. This double-step-index fiber profile is used to confine pump light within the fiber waveguide while featuring a high extinction ratio from the incorporated stress rods. The method used for sustaining a set polarization state is outlined in Section 2.5.3. In DC fibers, the cladding is designed to effectively guide high-power pump, however, for efficient coupling into the fiber core, there must be sufficient interaction of pump light with the fiber core. In Figure 11, a diagram is provided that shows the ability for stress rods to contribute towards the coupling of pump power in skewed optical rays that may otherwise remain unabsorbed.
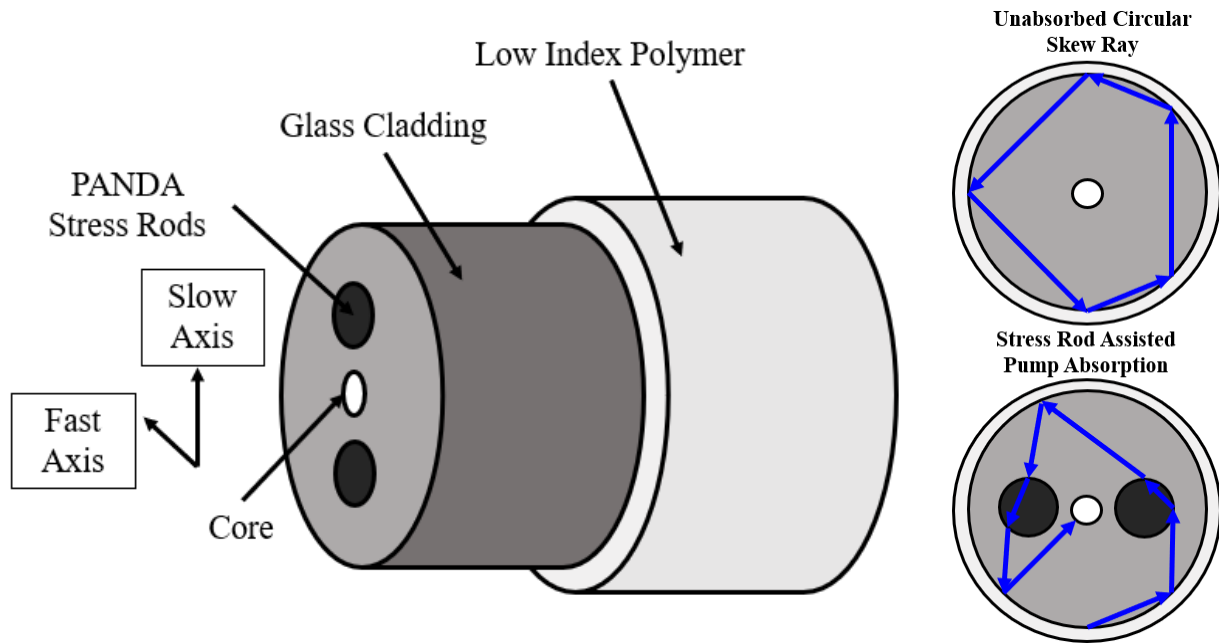
Figure 11: [Left] Double cladding polarization maintaining (DC PM) fiber with a low index polymer coating [23]. [Right] Stress rod assisted pump mixing for efficient pump power coupling.

2.5.2 Polarization Maintaining Fiber

In PM fiber manufacturing, a modified glass material is placed symmetrically to the fiber core within the heated fiber preform. When the fiber is drawn out, the modified material forms rods that run along the length of the fiber within the fiber glass cladding. This material is designed to have properties that apply stress to the fiber core when they cool. The stresses are applied in a way that induces birefringence, developing axes of ordinary and extraordinary refractive index in the fiber core. Electromagnetic waves propagating down the fiber will encounter the different indices of refraction depending on their orientation within the fiber core. This creates an effect where the linear polarization of the traversing signal is maintained regardless of any extrinsic stressors that are applied on the fiber from bending and straining. This method describes the processing of Panda PM fibers which will be used in the development of the Yb-doped MOPA fiber laser; however,

other fiber profiles exist that accomplish the same task. Alternate fiber profiles are provided in Figure 12.
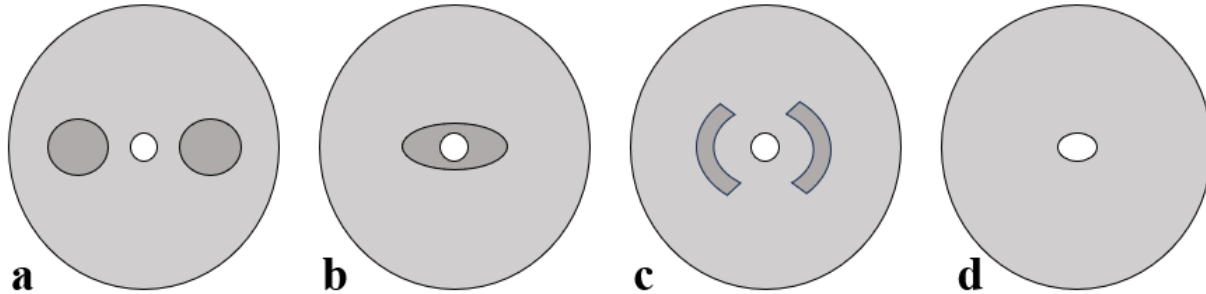
Figure 12: PM fiber designs include **(a)** those with circular stress rods in the cladding, also known Panda PM fibers, **(b)** those with an elliptical stress-applying member surrounding the core in the cladding, **(c)** those with bowtie stress rods, and **(d)** those with an elliptical core, from Yablon [55]

For Panda PM fibers, a strong birefringence effect is induced within the fiber with a slow axis developed in line with the two stress rods and the fast axis orthogonal to it. Light polarized along the slow axis experiences a higher index of refraction and travels more slowly than light polarized along the fast axis. Since light can be transmitted in both axes, PM fibers cannot act as linear polarizers. Instead, they are constructed to have high extinction ratios, >20 dB/m. This is a measurement of the ratio of light that transfers into other polarization states per meter of fiber that light travels.

When a fiber is bent or strained, small variations in the birefringence, observed by the signal, are induced. These variations can induce changes in the quality of the signal due to intermodal coupling. The variations vary with wavelength and increase proportional to the bending, twisting, and heating the fiber is subject to. PM fiber is constructed so that there is an internal stress applied that is magnitudes greater than the extrinsic stresses that a fiber is subject to in ordinary use. This

keeps the birefringent properties of the fiber relatively stable and helps to maintain a high-quality signal that retains its polarization, coherence, and modality over the length of the fiber.

2.5.3 Passive Fiber Components

Passive fiber components are optical devices with fiber coupled inputs that serve particular functions when integrated into a fiber system. They do not require external application of energy, and instead function independently when placed along the optical path of propagation. In the case of building a Yb-doped MOPA fiber laser, the passive fiber components that are used include isolators, pump combiners, a cladding light stripper, FBGs, and a circulator.

All devices are obtained from industry sources and come with set operating specifications, except for the cladding light stripper which was constructed in lab. This section provides context on the judgment and selection of each device utilized in the construction of the Yb-doped MOPA fiber laser. The components are listed in Table 1, and their manufacturer specifications, where available, are also provided.

Table 1: Passive fiber component operating specifications.

Passive Fiber Device	Center Wavelength and Range (nm)	Maximum CW Input Power (W)	Max Insertion Loss (dB)	Min Extinction Ratio (dB)
Isolator	1080±15	20	1	25
(2+1)x1 Pump + Signal Combiner	1020-1080nm Signal 780-1000nm Pump	50/port	0.5 Signal	20
Circulator	1064±20	20/port	0.78 (Port 1-2)	23 (Port 1-2)
			0.57 (Port 2-3)	26 (Port 2-3)
Volume Bragg Grating	1064±0.25	-	-	-
Cladding Light Stripper	-	-	-	-

Fiber optic isolators are used to block backwards propagating light in a fiber system which may damage the seed or pump laser diodes or contribute to internal instabilities, such as free lasing. They instill unidirectional propagation by way of Faraday rotators and polarization dependent free-space elements.. Similar to isolators, circulators utilize a mixture of Faraday rotators and free space polarization dependent optics such that light entering one of the three ports exits out of the subsequent port. As a result, forward propagating light entering port 1 exits from port 2 and light that may be back reflected, incident on port 2, will exit on port 3, and so forth, depending on the design of the component. The circulators are implemented to allow for the sampling of reflected optical energy from later amplification stages that will be added to this YDFL.

The pump combiner combines multiple input fibers into a singular output fiber. It confines pump power into the cladding of the output fiber, making cladding pumping of subsequent active fibers possible. The pump fibers are multimode and fuse into the internal cladding of the output fiber, whereas the signal fiber core is paired to the output core, one-to-one. Cladding light strippers are used to remove excess pump light from the fiber cladding. The fiber cladding is exposed, and a high index polymer is applied to it so that section of the fiber loses its waveguiding properties.

A schematic of the input/output ports of each external passive fiber component is provided in Figure 13. FBGs are different in the sense that they appear internally within a fiber waveguide. The internal fiber material is exposed to an intense UV source to periodically vary the internal index of refraction profile of the fiber in such a way that a Bragg grating is produced within the fiber core. This grating structure allows for wavelength selection and is present at the output fiber coupled ports of the seed and pump diodes.
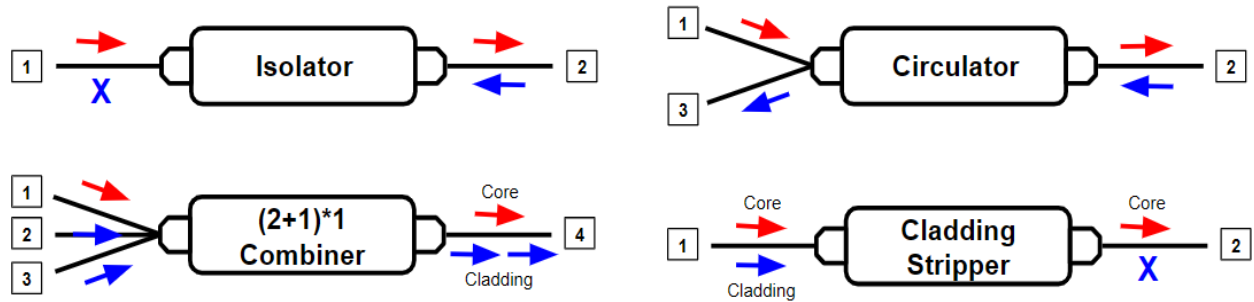
Figure 13: Schematic of fiber coupled passive devices.

Each device has an operating wavelength condition where the device is most effective at performing its function. The devices are selected for use at the Yb-doped MOPA fiber laser signal and pump wavelength, 1064 nm and 976 nm. Only the pump combiner is expected to process 976 nm light. In addition to the wavelength condition, each device also features a recommended maximum average input power for CW operation. Operation at powers greater than this may damage the fiber device.

The fiber isolator, pump combiner, and cladding light stripper feature insertion losses and minimum extinction loss ratios, measured in decibels. The insertion loss is a measurement of the fraction of input power that is lost as optical energy traverses the component. It is gained from the following equation:

$$dB = 10\log\left(\frac{P_{Out}}{P_{In}}\right)$$

The extinction ratio is a measurement of the polarization maintainability of a component. The values listed show the maximum ratio of power that is interchanged between polarization states within the device. The devices chosen feature relatively low, but non-negligible, insertion losses (<1 dB) and high extinction ratios capabilities (>20 dB) making them ideal for signal power and

polarization preservation through various stages in the fiber laser system. The insertion losses will be periodically checked against the manufacturer specifications throughout the laser's construction to ensure the devices are functioning properly.

CHAPTER 3: LASER DESIGN & ENGINEERING

This chapter summarizes the work invested into the design, construction, and characterization of the ytterbium fiber MOPA laser system. Industry standards for fiber processing are combined with techniques developed in lab to ensure optimal performance, reliability, and safety of the laser system. The engineering considerations investigated, combined with the data collected throughout the laser's construction, are verified with theoretical expectations serving as a proof of concept, supporting the validity of this work.

3.1 Laser Architecture

The MOPA laser architecture in Figure 14 is constructed to develop a low power, 366 mW, narrow linewidth, 59.1 GHz, seeding signal at 1064 nm to higher power (16.4 W) while maintaining the initial signal characteristics. It consists of three separate laser diodes: a seeding laser diode to generate the leading optical signal and two mid-power (10 W, 60 W) pump diodes to pump the Yb-doped active fiber at 976 nm and scale the output power of the 1064 nm signal.
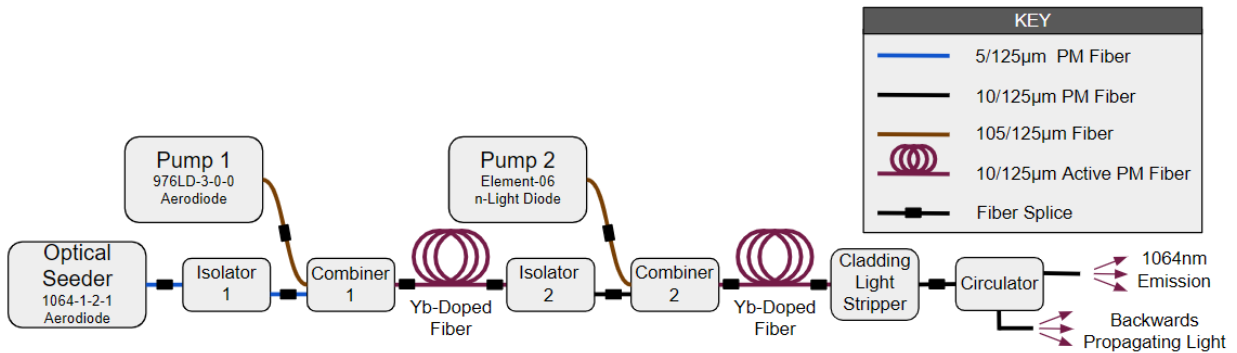
Figure 14: Ytterbium doped fiber MOPA architecture. Two independent Yb-fiver amplification stages are connected with intermediary components to generate a power amplified signal while minimizing instabilities.

Each of the individual blocks represents an active or passive fiber component that serves a unique purpose in the development of our system. The isolators are implemented to prevent backwards propagation of optical energy. The pump combiners merge the signal and pump inputs into the active fiber. The cladding light stripper is used to remove any excess pump light that may be present at the end of the second amplifying fiber to prevent damage to the circulator, which is not graded for 976 nm. Lastly, the circulator is included to provide the operator with a sampling point for backwards propagating light that may develop in further amplification stages this system will be attached to in the thermal blooming experiments.

Two separate stages of Yb-doped fiber amplifying media are utilized to limit ASE generation. The first amplification stage consists of 2.5 m of Yb-doped fiber and the second stage utilizes 4.5 m. Relying on a single stretch of active fiber would result in the oversaturation of the gain media without sufficient power from a driving signal to encourage a particular lasing mode. By separating the amplification stages, we can maintain an adequate seed-to-pump power ratio, reducing gain competition between stimulated emission at 1064 nm and the development of ASE from other transitions that are not properly stimulated.

The system is mounted onto a 15x18x0.5-inch water-cooled aluminum base plate with threaded holes to keep the diodes, active fiber, and fiber components secured and cooled during use. Fiber spools and mandrels are utilized for fiber management and a beam dump is integrated for back reflected light emitting out of the unused pump combiner inputs and the circulator back reflection sampler, modeled in Figure 15. Figure 16 displays the actual layout of the fiber laser system.
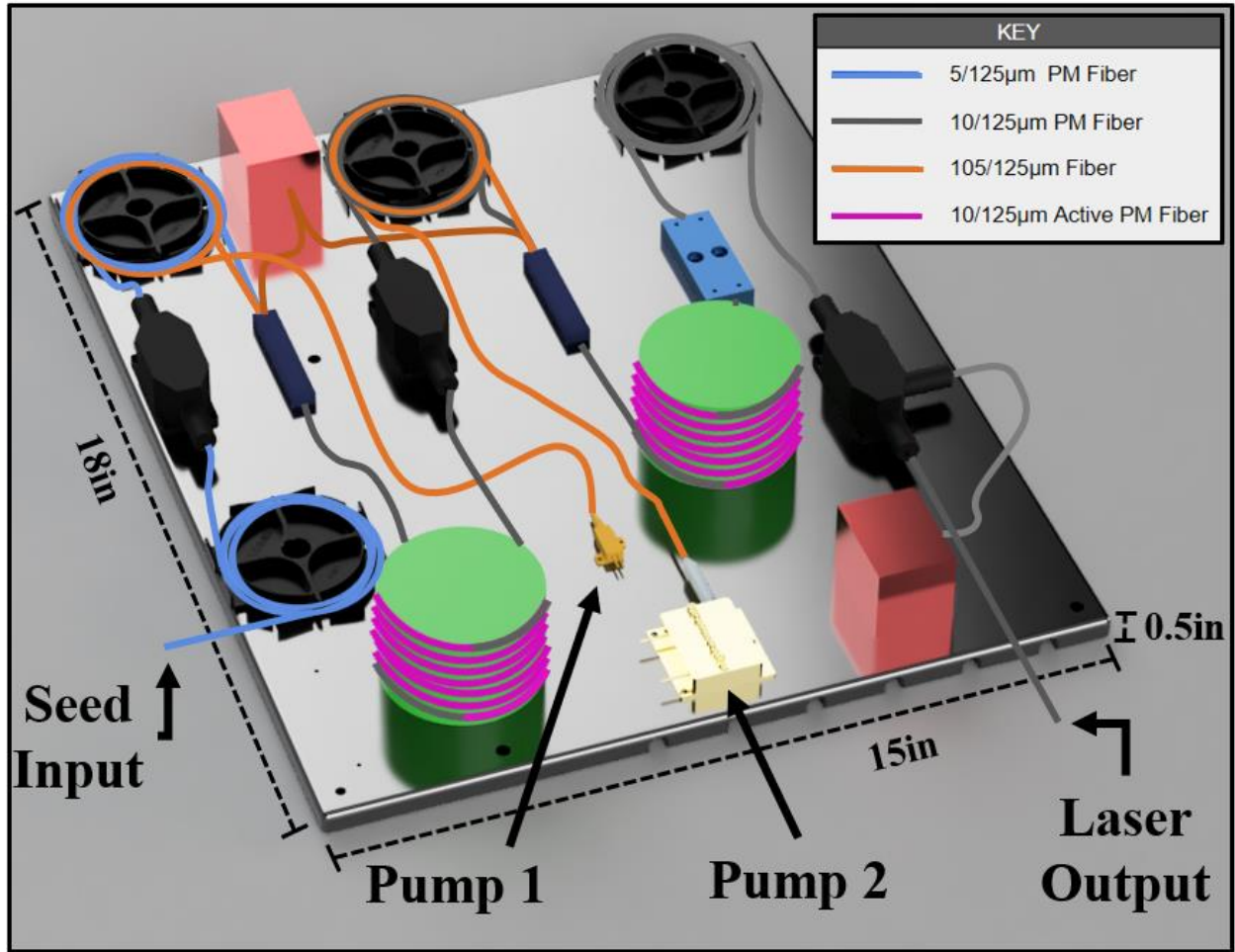
Figure 15: Modeled layout of the ytterbium doped fiber MOPA depicting fiber management techniques and various types of fiber.
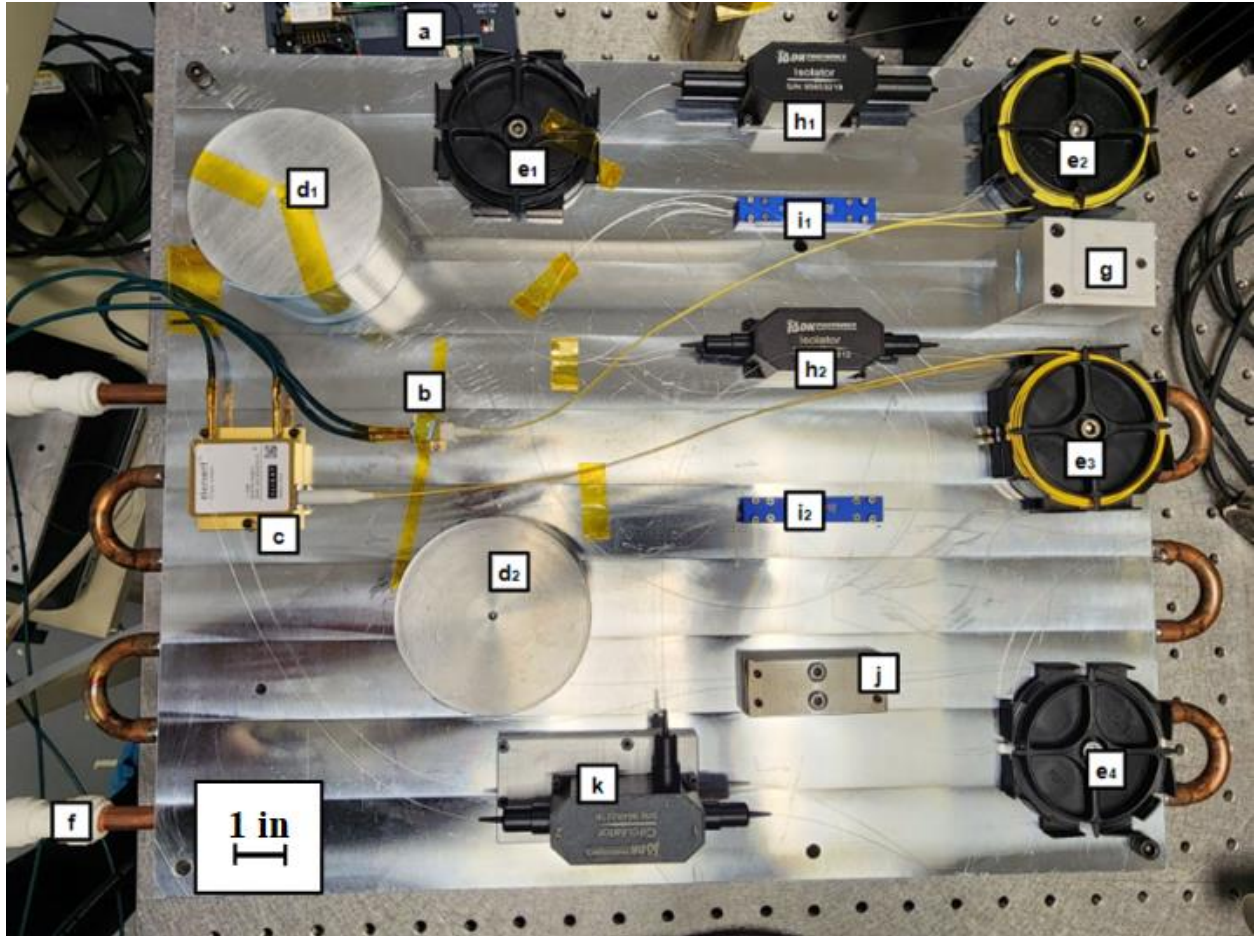
Figure 16: Physical layout of ytterbium doped fiber MOPA on aluminum base plate. (a) Seed laser diode. (b) Pump 1 laser diode. (c) Pump 2 laser diode. (d) Fiber mandrels for active fiber cooling. (e) Fiber spools for passive fiber management. (f) Brass tubing for water cooling. (g) Beam dump for unused fiber ends. (h) Isolators. (i) Pump combiners. (j) Cladding light stripper. (k) Circulator.

3.2 Fiber Processing

In the construction of this fiber optic system, multiple waveguides, each serving their own purposes, are coupled into one another to ensure efficient signal pass over. In the efforts of building a continuous fiber laser system, the output of one fiber is bound onto the input of another in a process known as splicing. Fiber splicing, however, involves a lot of meticulous preparation for processing that can become more complex depending on the fiber properties. These steps will be

outlined in this section. Prior to the splice taking place, the involved fiber ends need to be stripped, cleaved, aligned, and recoated.

Both the multimode and single mode fibers utilized in the construction of the low power Yb fiber laser feature a double clad structure. A centered inner core is covered by a glass cladding of lower index followed by a polymer coating of even lower index. The outer polymer layer acts as a second cladding, so it is important that this layer does not become damaged. This polymer coating is stripped in preparation for fiber splicing. The polymer must be removed prior to splicing because it does not melt and bind at the same temperatures needed for the glass core and cladding which are much more similar in their thermal properties. The temperatures required for fusion splicing range from 2000 to 3000°C. The low index acrylate, used to coat most fibers, melts at approximately 150°C [56]. In the engineering of this fiber laser system, stripping of the fiber polymer outer layers is done manually using a razorblade that is slid across the fiber cladding surface.

After stripping the polymer, the exposed cladding is wiped clean with lint-free wipes to remove any dust and remnant particles that may remain from the fiber strip. If further cleaning is necessary after cleaving the fiber, an ultrasonic rinsing in an alcohol bath containing methanol may be performed. Figure 17 depicts a cleaved fiber end before and after thorough cleaning. Note that the following figures of PM fibers do not accurately depict the fiber core diameter due to the presence of the fiber stress rods.
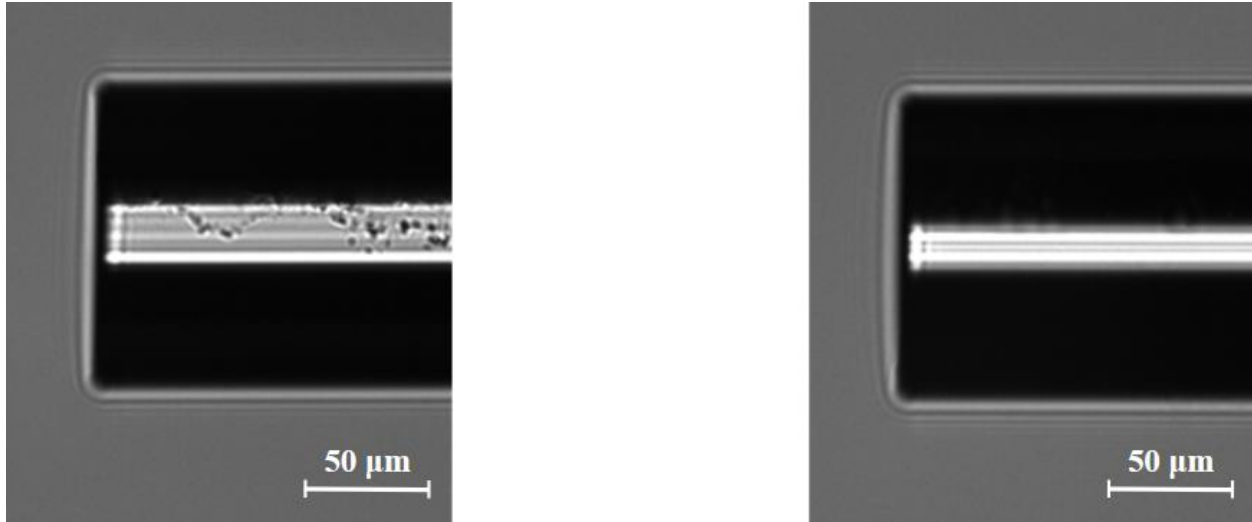
Figure 17: (Left) Poorly cleaned 10/125 µM PM fiber with dust and polymer residue left on the fiber glass cladding after mechanical razorblade stripping. (Right) A separate 5/125 µM PM fiber after wiping with a Kimtech wipe and an ultrasonic bath in alcohol.

After cleaning, the fibers are cleaved using an electronic cleaving device. To do this, both ends of the fiber are tensioned and a diamond sharp edge scribing tool is repeatedly struck against the exposed fiber cladding until a fracture is created. The number of presses and amount of tension applied must be optimized for each individual fiber type and diameter. Accurate cleave angles were found when the fiber was tensioned 210 g for the pump diode LMA 105/125 µm fiber, the 5/125 µm PM, and 10/125 µm PM fibers. Defects are common. Cases where the fiber end is left chipped or improperly angled, result in the cleave needing to be repeated. Improperly cleaved fiber ends increase core distortion and loss experienced at the spliced joint [57, 58].

To increase the chances for a successful splice, fiber ends were prepared to have a clean cut and angle < 0.4°. Angled cleaves are sometimes desired. Cases where the output of a fiber is to be sampled required cleave angles between 4 and 6° to minimize chances for internal reflection at the

fiber end [32]. Figure 18 showcases the angled and flat cleave cases utilized throughout the construction and characterization of the fiber laser.
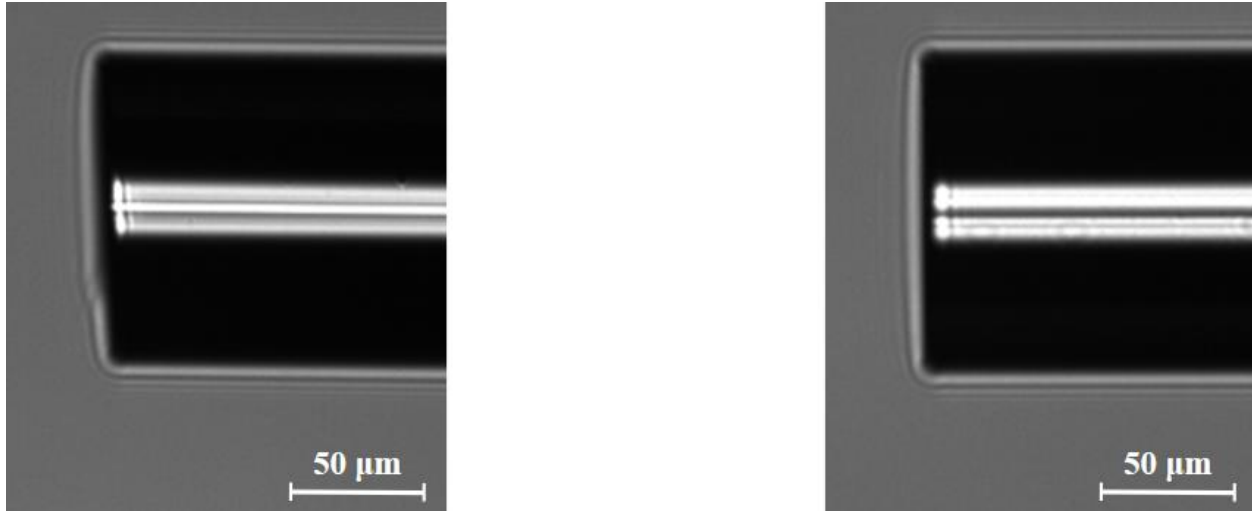
Figure 18: (Left) Angle cleaved 10/125 µM PM fiber prepared for efficient outcoupling of the optical energy ($4° > \theta > 6°$) to minimize risk for self-pulsing and self lasing [53, 58]. (Right) Flat cleaved 10/125 µM PM fiber prepared for splicing ($\theta < 0.4°$).

Upon preparing both fibers for splicing, alignment of the fiber ends is performed using the Fitel Ring of Fire Fusion Splicer. The prepared fibers are loaded into chucks of the appropriate diameter to be held in place and positioned. The Fitel Fusion Splicer features optical diagnostic equipment so that the user may observe the fiber ends for cleanliness and uniformity. This is where Figures 17-18 are retrieved. A check of the relative angle between the two fibers was also obtained. The flatter the surface, $< 1°$ angle in the X and Y planes relative to each other, the more likely the outcome a successful splice becomes. In PM fiber, there is an added variable of aligning the internal stress rods running along each fiber. Once aligned, the fibers are pushed together between three electrodes, a few millimeters across, and an electrical arc discharge is applied across them through the air to heat and melt the fiber tips together.

Due to the variable nature of splicing, each splice must be tested for imperfections. Common imperfections include the misalignment of the internal stress rods in PM fiber and the development of bubbles within the fiber from poorly cleaved fiber tips. To test each splice, a stress test is performed, bending the fiber to extreme radii of curvature. If the fiber breaks at the location of the splice, then the fiber processing steps are repeated. Additionally, if the fiber passes the stress test, a test of power loss is performed. Splices that result in significant drop in the laser output power through the splice (>0.3 dB) are also repeated. Power loss greater than this indicates leaking or heating at the fiber splice point which may be catastrophic at higher powers. Figure 19 showcases various fiber splices attempted in this laser's construction.
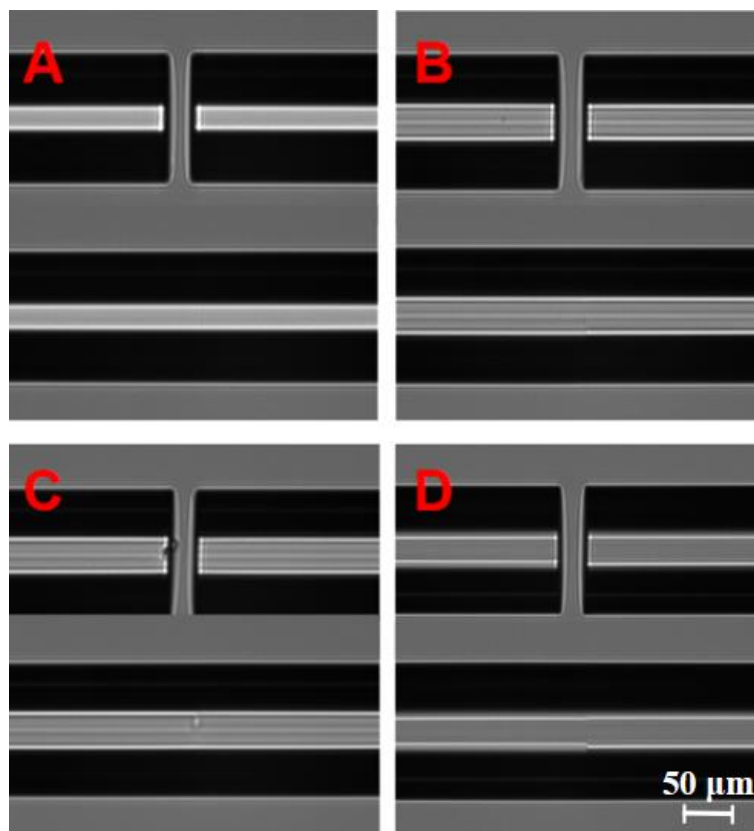
Figure 19: (A) Satisfactory 105/125 µm LMA fiber splice. (B) Satisfactory 10/125 µm fiber splice. (C) Unsatisfactory 10/125 µm PM fiber splice due to imperfection at left fiber end. (D) Unsatisfactory 10/125 µm PM fiber splice due to misalignment of PM fiber stress rods.

Splices C and D were eventually redone due to poor quality. Note the extremely small visual identifiers of a bad splice. This is why the tests mentioned earlier are so necessary to perform as they provide a better indicator of splice quality. After satisfactory splicing, a liquid polymer of appropriate index is applied over the stripped portion of fiber and is UV-cured to a solid coat.

A list of all splices in the construction of the Yb-based MOPA fiber laser are provided in Table 2.

Table 2: All finalized splice specifications in Yb-doped MOPA fiber laser. PM denotes the polarization maintaining signal carrying fibers. MM denotes the multi-mode fibers coupled onto the pump diodes.

Splice #	Description	Relative Angle (°)	Splice Program & Type	Arc Power	Gap (um)	Estimated Loss (dB)	Estimated Extinction Ratio (dB)
1	Seed > Isolator 1	0.54	No. 16 PM-PM	39	23	0	44.61
2	Isolator 1 > Comb 1	0.21	No. 16 PM-PM	36	23	0	40.17
3	Pump 1 > Combiner 1	0.62	No. 5 MM-MM	39	20	0	-
4	Combiner 1 > Yb-Fiber 1	0.36	No. 16 PM-PM	39	20	0	39.66
5	Yb-Fiber 1 > Isolator 2	0.69	No. 16 PM-PM	39	23	0	44.45
8	Isolator 2 > Combiner 2	1.43	No. 16 PM-PM	39	21	0.01	44
9	Pump 2 > Combiner 2	1.31	No. 5 MM-MM	42	21	0	-
6	Combiner 2 > Yb-Fiber 2	1.03	No. 16 PM-PM	39	21	0	42.6
7	Yb-Fiber 2 > Cladding Light Stripper	1.27	No. 16 PM-PM	39	21	0.02	44.57
10	Cladding Light Stripper > Circulator	1.09	No. 16 PM-PM	39	22	0	43.76

All splices listed have been successfully stress tested and feature negligible losses, including those with relative angles exceeding 1°. Two separate splice programs were utilized: No. 5 and No. 16 for single mode polarization maintaining fibers and multimode fibers respectively. The Fitel Fusion Splicer was set to have an arc power of 39 units for fibers of 125 µm cladding diameters for optimal results. Each fiber is pushed 10 µm inward upon splicing, so a gap spacing of approximately 20 µm is required upon fiber positioning. For the PM fiber, an estimated extinction ratio of approximately 40 dB more than suits the polarization maintenance needs of the system.

3.3 Thermal Management of Diodes & Fiber Components

Due to the dependence many of the device components have with temperature in regard to their operating efficiencies, careful considerations were put into the thermal management of the fiber laser system. Laser diodes are known to release thermal energy during use and the active/passive fiber components used can also contribute to heat generation. As discussed in Chapter 2, rising laser diode operating temperatures contribute to spectral broadening and wavelength drift in their emissions to not center on areas where peak gain is acquired for the Yb-doped fiber. This section details the investigation of the thermal impact and the steps taken to minimize it throughout the laser's construction.

Central to the thermal management methods implemented in this design is the active cooling of the aluminum base plate on which all the system subcomponents are mounted. De-ionized water, chilled to 16.2°C, is pumped through the aluminum baseplate. To optimize efficient heat transfer between the base plate and active/passive fiber components, the components must be bound to the cooled plate with a thermally conductive material in-between. The diodes and passive fiber components often come encased in metallic casings that are excellent thermal conductors,

however, in direct binding to the aluminum baseplate, the metal-on-metal contact is typically imperfect and features pockets of air which acts as a thermal insulator between the two metals. For this reason, a test of various accessible thermally conducive materials is administered to optimize the heat transfer between the laser subcomponents and the baseplate.

The thermal conductivity tests administered features the layout displayed in Figure 20. A 10 W resistor is driven by a power source to generate heat into an aluminum plate. It is pressed into a second aluminum plate that is cooled to a set temperature, 16.2°C. A thermistor is used to measure the temperature in the top and bottom aluminum plates. Between the two plates lies a plastic thermal insulator with a height of 0.1016 mm and a 25.4 mm by 25.4 mm (1 x 1 inch) cutout. In the cutout, various thermal conductors are inserted and tested for thermal conductivity.
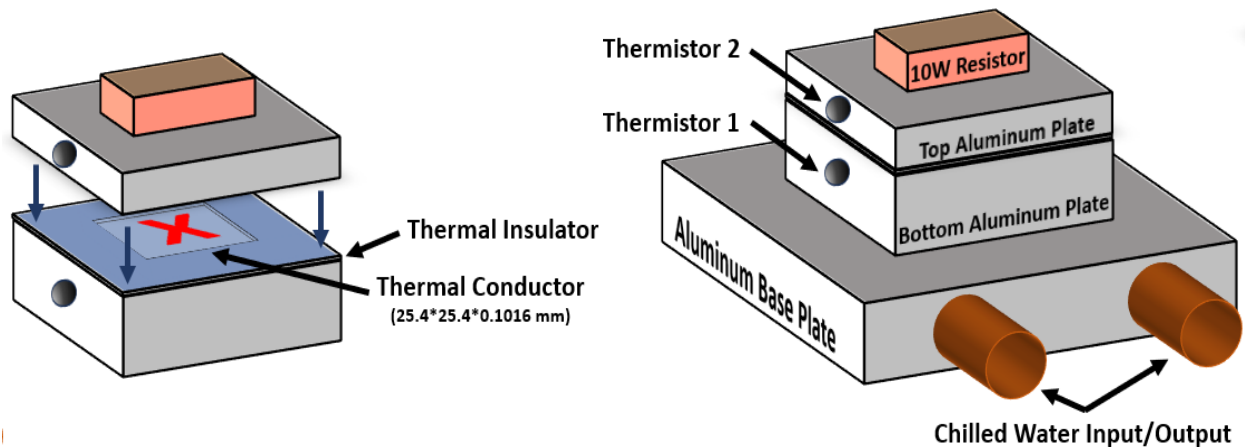
Figure 20: (Left) X marks the area where thermally conductive materials are applied. (Right) When the plates are pressed closed, the thickness of the plastic thermal insulator defines the height of the thermal conductor.

As a control, Figure 21 showcases the thermal exchange when no insulator or conductor is placed between the two plates.
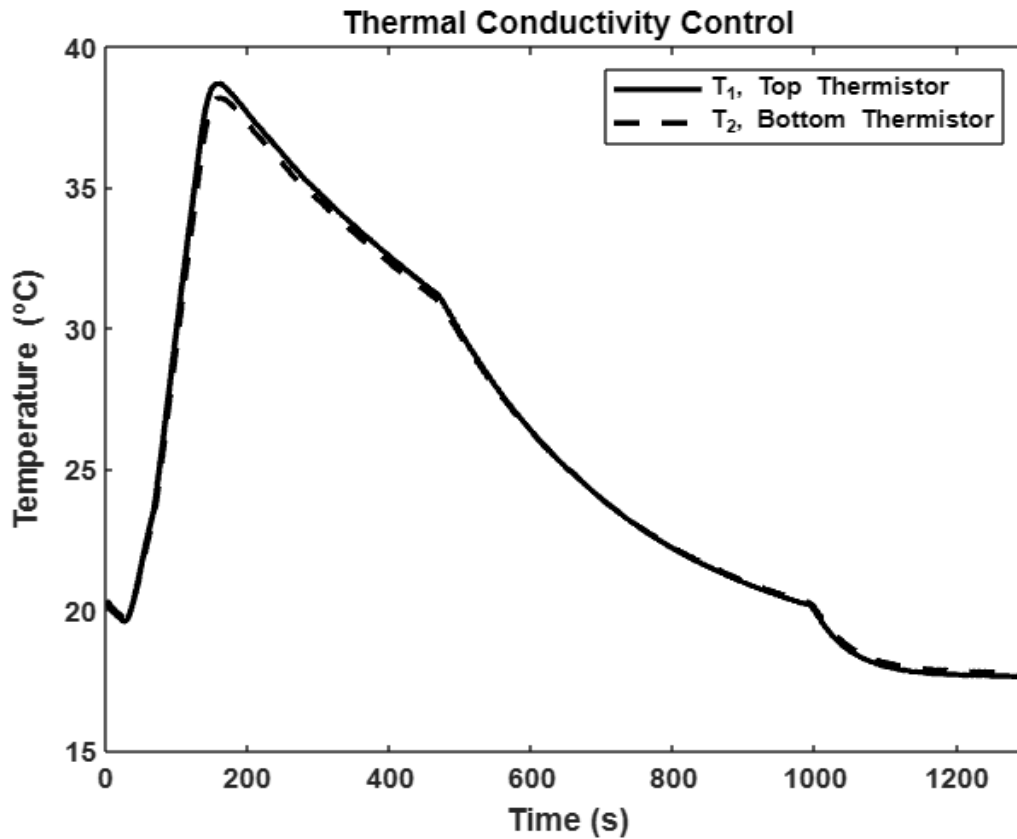
Figure 21: The resistor is driven, producing 10 W of heat at t = 20 s, raising the temperature of both plates to 38°C. It is powered off at t = 180 s and both plates fall to equilibrium at 17.8°C, slightly above the water temperature due to the influence of the surrounding room temperature.

The maximum operating temperature is determined to be 38°C with no external temperature control. This lies outside the manufacturer specified operating temperature for the laser diodes that will be used as pump sources in the construction of the fiber laser system. This justifies the need for investigation into thermal management methods as the heat generation of the pump diodes may very easily exceed 10 W.

The materials to be tested consist of thermal epoxy, a pink and blue thermal heat pad, carbon filler-based thermal paste, and a graphite pad. They were chosen for their general availability and use in industry for thermal management applications. Logging the change in temperature over time after

46

the resistor is driven for various conducting materials provides the following data, represented in Figure 22:
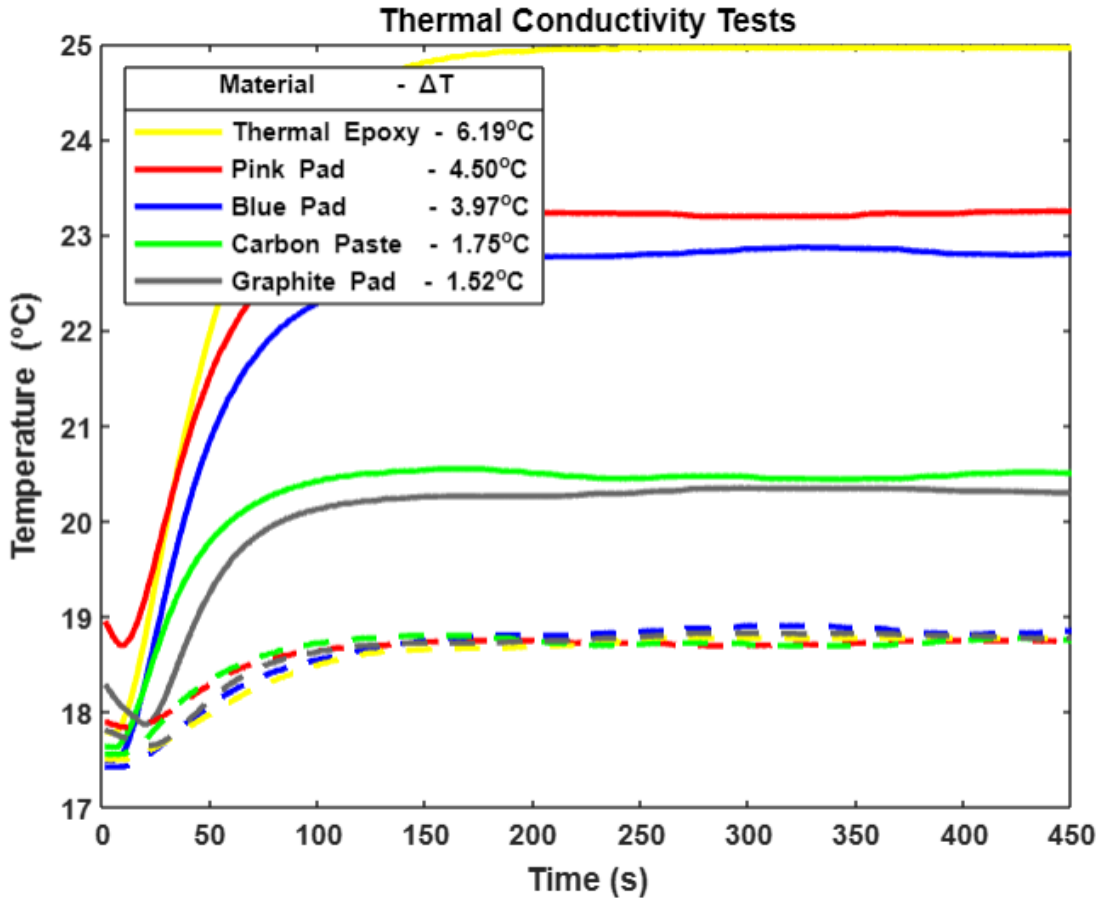
Figure 22: The temperature logs for various materials in the thermal conductivity test. The solid lines represent the data from the top thermistor and the dashed lines represent the data from the bottom resistor for t = 0 s to 450 s. Each material approaches a thermal equilibrium as the resistor is driven.

From the data presented in Figure 22, we can intuitively conclude that all materials provide some degree of thermal management, however the carbon paste and graphite pads provide the best support. The thermal conductivity of each material is determined by the following relationship:

$$K = \frac{Ph}{\Delta TA}$$

Where P is the power of heat generation, given by the resistor driven by substantial current, h is the height of the thermal conductor, ΔT is the difference in temperature between the top and bottom plates, and A is the surface area of heat transfer given by the square cutout. Using the data in Figure 22, the conclusion is further supported by the calculated thermal conductivity values, provided in Figure 23, with some error introduced by thermistor accuracy.
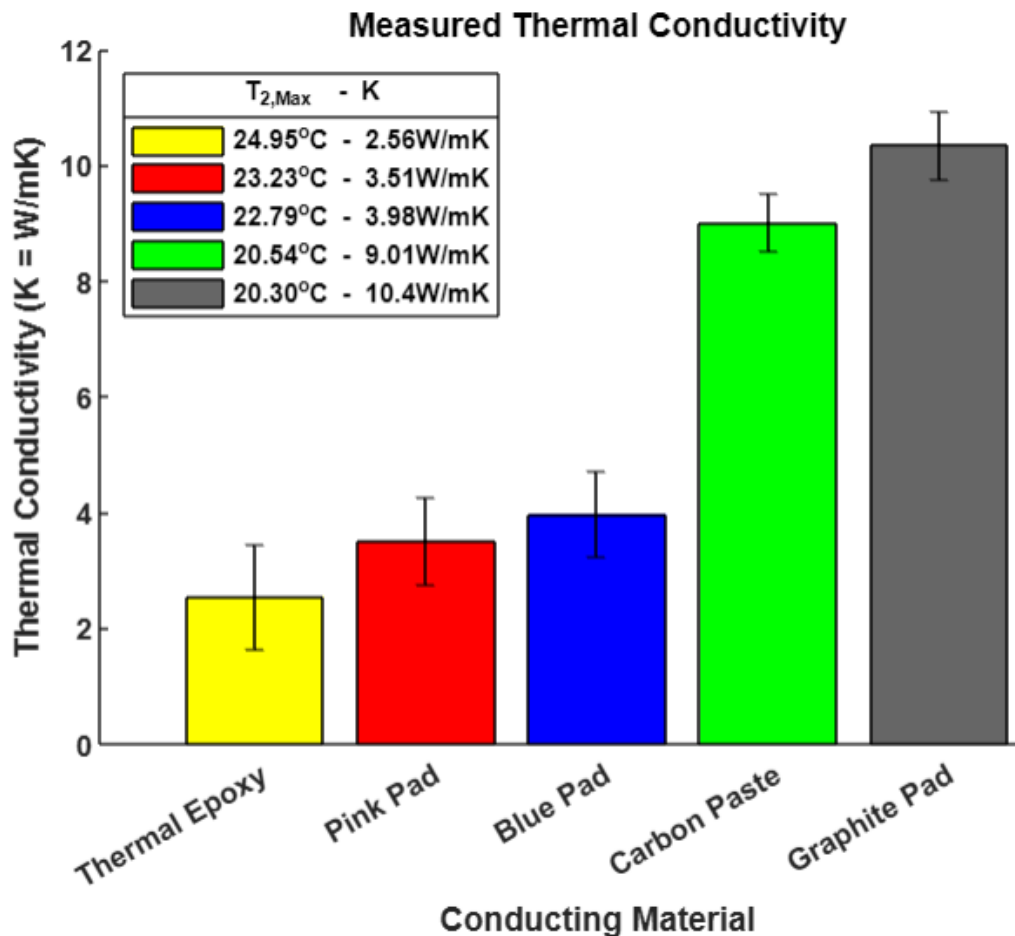
Figure 23: Calculated thermal conductivity of each tested material. The carbon paste and graphite pad feature thermal conductivities more than twice that of their counterparts.

Due to its molecular layered structure, graphite is best utilized to conduct heat over the length and width of its body as it may prove to be less effective for transferring heat through vertical thermal displacement. The graphite pad is used to cool only the second pump diode, in line with the manufacturer specifications, likely due to featuring a relatively concentrated hot spot that is small relative to the total diode package size.

The decision to secure the laser diodes and fiber components to the water chilled aluminum baseplate using the carbon paste as the heat transfer medium was decided as it is supported by the empirically gained evidence to be an efficient thermal conductor and it has a relative ease of use.

In addition to the cooling mechanisms implemented to dissipate heat, steps have also been taken to minimize the total amount of heat generated. Assuming that the semiconductor inefficiencies not contributing to heat generation are negligible, we can safely assume that the difference in the supplied electrical power to emitted optical output power, primarily contributes to heat generation. This difference can be measured. The laser diodes are driven by supplying a voltage across the diode input pins. The total supplied power to the diode is given by Ohm's Law:

$$V = IR$$

$$P = IV = I^2R$$

Where V is voltage, I is current, R is resistance, and P is power. Taking the difference of the electrical input power and the output optical power, provided by a power meter, provides the power loss contributing to heat generation. Assuming that the internal operating losses of the laser diodes remain constant, we find that the power input-output difference is heavily dependent on the resistivity encountered at the diode connector interface where the input power is supplied. Initially, alligator clips were used to connect the diodes to the power supplies. Sleeve connectors were used

to replace the alligator clips for maximized contact area between the power supply and the diode bias connector pins.

When the alligator clips were used to supply I = 9 A of current to the pump 1 laser diode, a potential difference of V = 2.23 V, measured through the function generator, was required. The measured optical output power was 6.06 W, resulting in a power differential of $\Delta P = IV - 6.06$ W = 14.01 W which we can assume corresponds linearly with heat generation. The operating temperature of the diode operating in this regime was measured to be 23.9°C. With the new connectors, 9 A was supplied with only a 2.01 V potential supplied across the diode pins. The output optical power was measured at 6.77 W, resulting in a new power differential of 11.32 W. The operating temperature of the diode operating package was measured to be 19.4°C. Optimizing the connectors provided greater operating efficiency of the laser diode.

To support the conclusions gained from the thermal conductivity experiments and the relating considerations on thermal management, including proper diode forward biasing, the pump 1 diode was operated in two cases. In the first case the laser diode was scaled to near-maximum output power without the active cooling from the base plate or modified connectors. In case 2, the laser diode was actively cooled by being secured to the base plate with a thin layer of carbon paste and was biased using sleeve connectors. The laser output power and diode packaging temperature were logged in each operating regime and is presented in Figure 24.
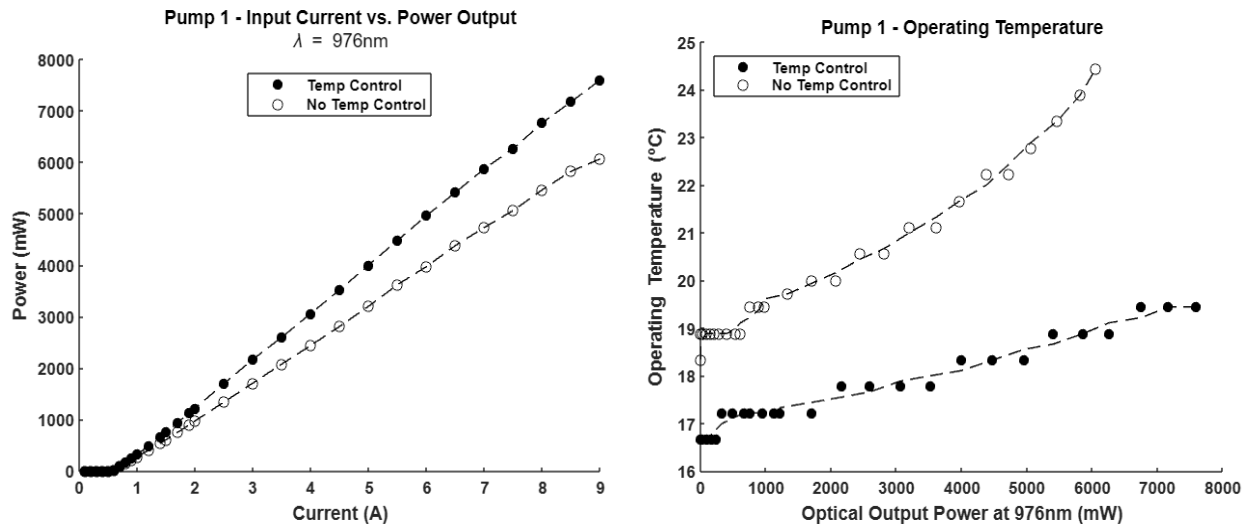
Figure 24: Characterization of diode output power at 976 nm with and without thermal generation and displacement considerations.

It is apparent that the modifications made drastically aid in maintaining a consistent operating temperature for the laser diodes. Due to the change in operating temperature and the connectors utilized, the measured slope efficiency for the pump 1 laser diode increased from approximately 0.72 W/A to 0.81 W/A, yielding a change greater than 25% in output power of the diode when driven at 9 A.

Additionally, knowing that the center wavelength of the laser diode emission is also temperature dependent, according to the manufacturer specifications, these changes prove even more necessary as it is crucial that the pump power remains near the 976 nm absorption band for Yb^{3+}. The total change in temperature, ΔT, between the cooling and non-cooling case for the pump 1 diode was approximately 6°C. The pump 1 and pump 2 laser diodes feature center wavelength temperature coefficients of 0.02 nm/°C and 0.01 nm/°C. The center wavelength drift and FWHM broadening were measured experimentally for the pump 1 diode and are presented in Figure 25. Additional diode output characteristics are provided in Chapter 4.
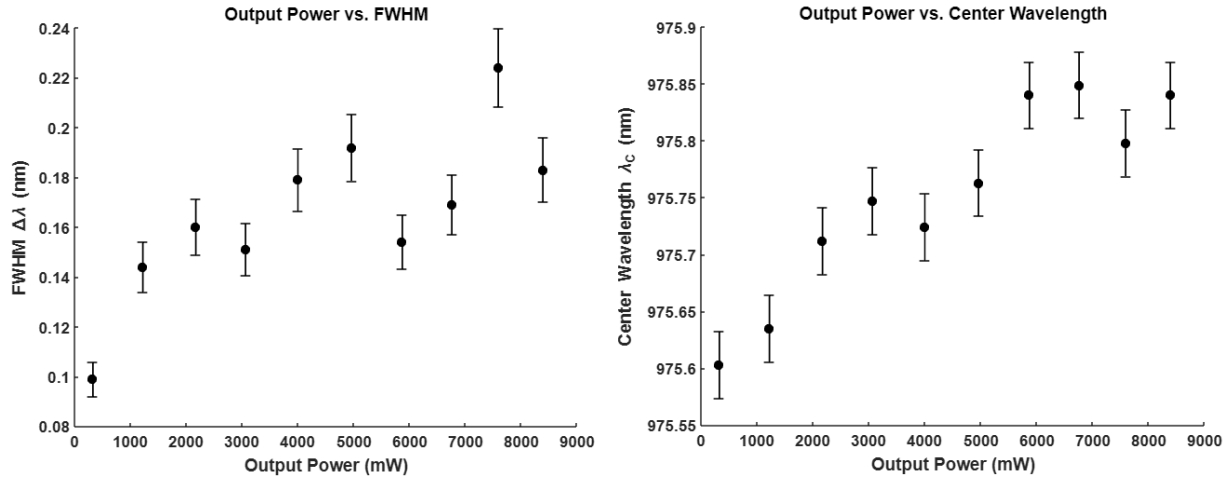
Figure 25: [Left] Pump 1 FWHM vs. output power and [Right] center wavelength vs. output power with temperature control considerations.

<div align="center">

3.4 Intermediate Beam Sampling Methods

</div>

To ensure each stage of the Yb-doped MOPA fiber laser was operating satisfactorily, the optical emission of the laser after every spliced component is sampled for spectral quality and power. Although beam sampling may prove trivial at times, requiring no more than direct coupling into measurement devices straight out of the fiber end, sometimes more complex methods are required to accurately retrieve data critical to characterizing the development of the laser system.

Standard pyroelectric heat-based IR power meters are utilized to characterize optical output power. Because the power meters operate generally within the UV-VIS-IR range, they are unable to accurately differentiate between optical emissions within a few nanometers, spectrally, of each other. For this reason, dichroic mirrors are used to spatially separate the emissions where both 1064 nm signal and 976 nm pump emissions are known to be present.

To collect spectral data at each measurement point, an Optical Spectrum Analyzer (OSA), with an accompanying fiber coupled input, from Anritsu Corporation is used. Because the OSA has a

maximum intensity load where powers in excess may cause damage to its internal workings, no more than 1 mW of average CW power is coupled into the OSA fiber input at any given point in time. For this reason, in addition to the raw fiber ends unable to be connected end-to-end with the OSA fiber connectors, the output of the laser system is coupled through an array of free-space optics. Figure 26 depicts the optical setup utilized for efficient beam sampling, allowing for the retrieval of power and spectral data simultaneously.
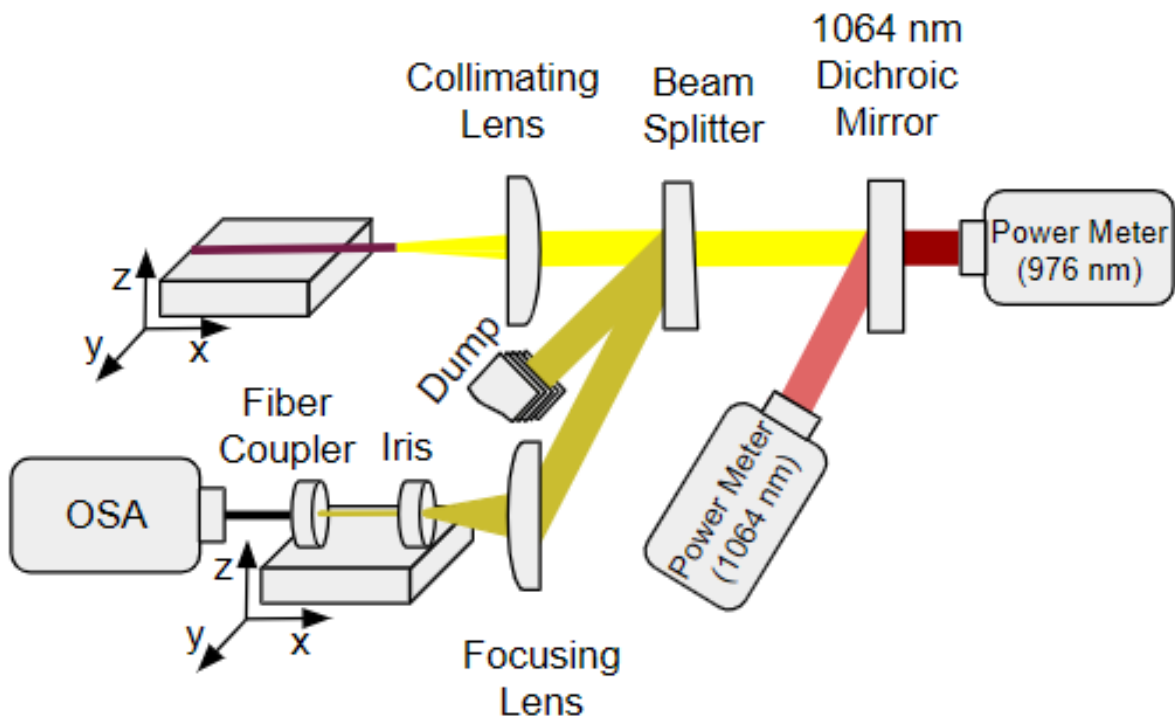
Figure 26: Optical setup utilized for simultaneous retrieval of optical power and spectral quality measurements.

The optical setup outlined above, although depicted sampling the output of the first amplification stage, is used to characterize the laser at various stages of its development. A fiber launch stage is positioned in front of a collimating lens on a 3-axis translation fiber launch stage for spatial fine tuning. A beam splitter is used to redirect a portion of the incident light towards the OSA so as to

not exceed the OSA's damage threshold. The beam splitter reflects 4% of the incident light on the front and back surfaces, allowing 92% of the total incident light to be transmitted through. The redirected collimated light is focused on the end facet of the OSA fiber coupler. After the beam splitter, the transmitted light is split by a dichroic mirror that is tuned to reflect 99% of incident 1064 nm light toward the signal power meter. The pump light is transmitted through the dichroic mirror with minimal loss and is measured by the pump power meter. This allows for the measuring of the signal and pump emissions independently. The values of power recorded are later corrected for the losses experienced at each free space optical device. This optical measurement method is used to retrieve the intermediary and final characterizations of the YDFL, presented in Chapter 4.

CHAPTER 4: LASER CHARACTERIZATION

4.1 Laser Diode Characterization

The characterization of the optical input diode, used as the master oscillator, and the supporting pump diodes is critical to the development of the Yb-doped MOPA fiber laser system. Since they serve as the independently variable sources, they must be carefully characterized so that the performance of subsequent active and passive fiber components in the system may also be measured. This section provides a general description of the technical specifications of the laser diodes used and the rationale behind their use and integration into the Yb-doped MOPA fiber laser. The in-depth characterization of each diode retrieved in lab is compared against the manufacturer specifications. These characterizations include the diode P-I curves and spectral outputs. All measurements recorded in this section are obtained from emissions sampled directly out of the diode coupled fiber ends, prepared with 4° cleave angles.

4.1.1 Seed Diode

The laser diode utilized to inject the seeding signal is the 1064-1-2-1 Aerodiode. The code references the emitted center wavelength (1064), then diode type (1), followed by the driver type (2), and form factor (1). This laser diode acts as the master oscillator of the system. This laser diode emits a continuous wave single mode beam with high spectral purity centered at $\lambda_c = 1064.871$ nm. It contains a built-in narrow emission spectrum FBG allowing it to maintain an emission full width at half maximum (FWHM), λ_{FWHM}, of 0.223 nm with a maximum output power, up to of 394 mW, according to the manufacturer specifications. The polarization state of the emitted beam is linearly aligned to the slow axis of the coupled Nufern PM980 fiber that comes prepackaged to the diode output facet. The diode is driven with a 12 V Butterfly 1064 Aerdiode

CW laser driver with a maximum operating current of 800 mA. The diode driver inputs are digitally adjusted. The diode contains an integrated thermoelectric controller (TEC) unit set to 35°C. The in-lab characterization details are provided in Figure 27.
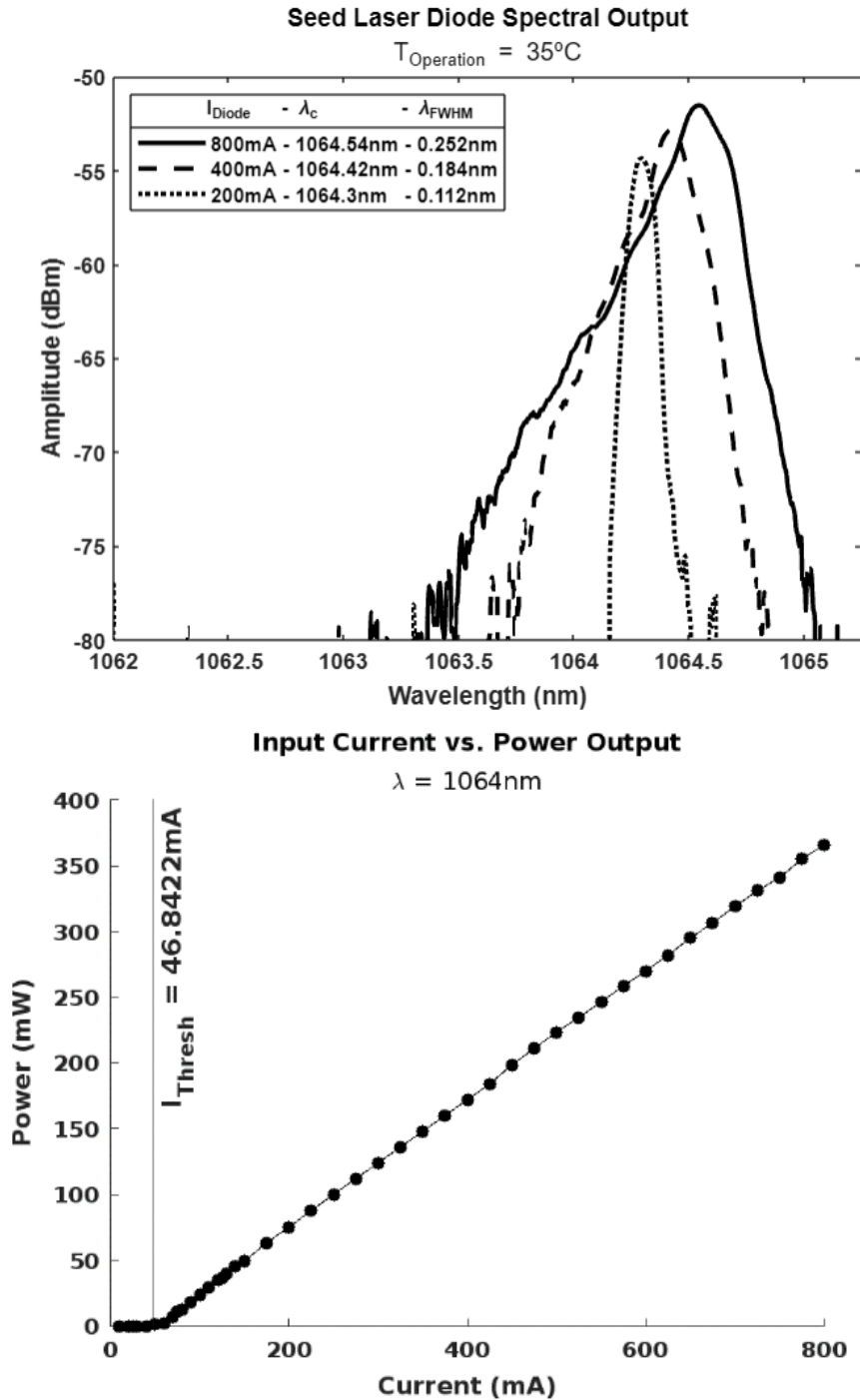
Figure 27: Seed laser diode characterizations. [Top] Seed spectral data. [Bottom] Seed P-I curve.

The seed diode maintains a fairly narrow linewidth, $\lambda_{\text{FWHM}} < 0.252$ nm, as it is in the sub-nanometer range. The spectral output remains stable over time and output power after 225 mW, indicating impressive spectral consistency, however, minimal broadening is observed at higher drive currents. The stability in the seeding signal is sufficient for continuous gain saturation in the MOPA amplification process. The seed diode features a 0.49 W/A slope efficiency and will be run at maximum output power, 800 mA for $P_{\text{Out}} = 366$ mW. So, a $\lambda_{\text{FWHM}} = 0.252$ nm and a $\lambda_c = 1064.54$ nm is expected when running the system for optimal amplification within the Yb-doped MOPA fiber laser system. It is run at the maximum output setting since greater signal power assists in maintaining lower levels of ASE.

4.1.2 Pump 1 Diode

The laser diode utilized to pump the first amplification stage is the 976LD-3-0-0 Aerodiode. This laser diode emits a continuous wave multimode beam centered at $\lambda_c = 975.5\pm0.5$ nm, and $\lambda_{\text{FWHM}} < 0.7$ nm, up to a maximum output power of 10 W, at 13 A drive current, according to the manufacturer specifications. The diode has a standard operating temperature range of 20-30°C. The diode also comes prepackaged with a diode-fiber combiner to a NA $= 0.22$ multimode 105/125 μm fiber. The in-lab characterization details are provided in Figure 28.
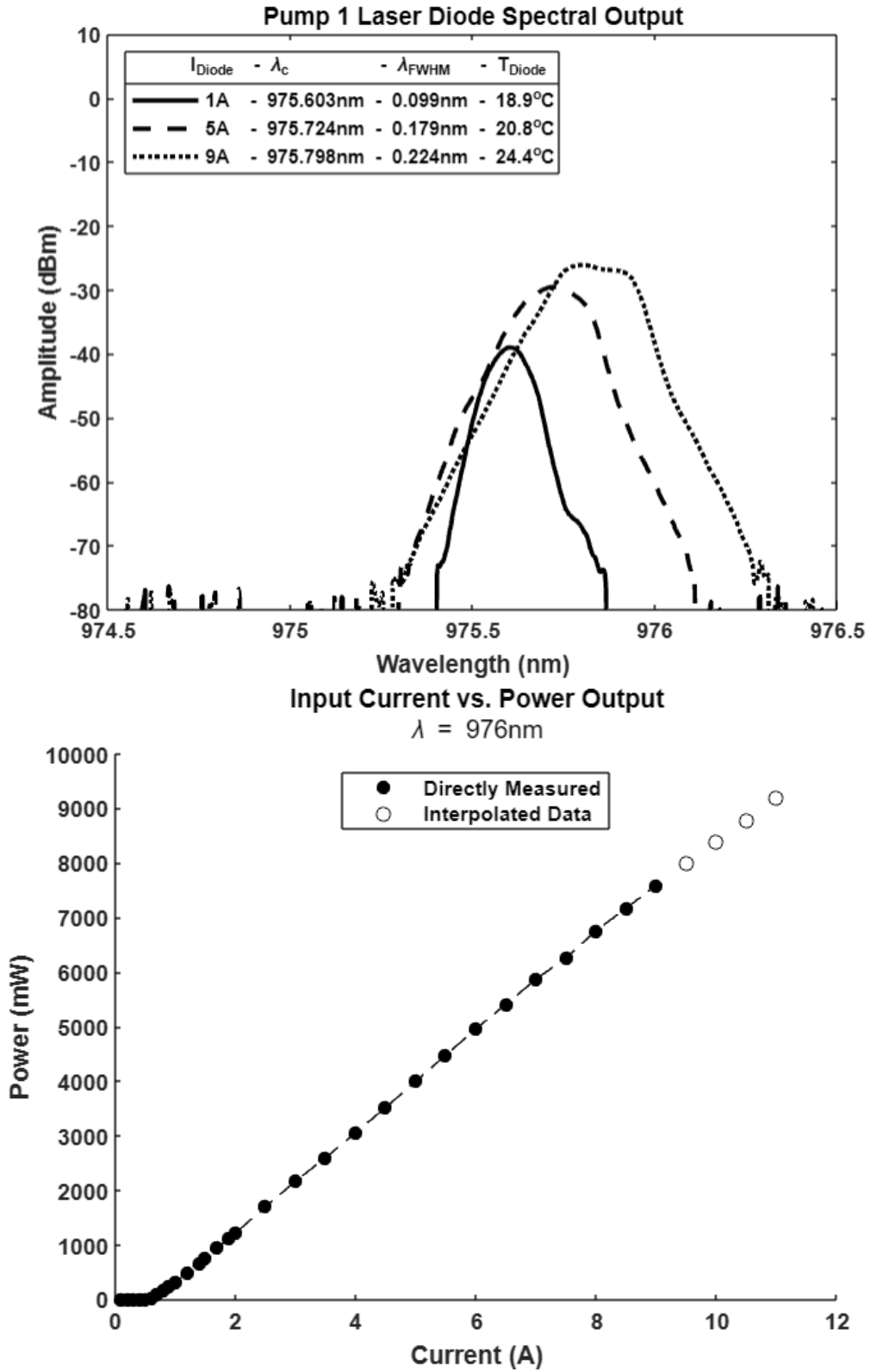
Figure 28: Pump 1 laser diode characterizations. [Top] Pump 1 spectral data. [Bottom] Pump 1 P-I curve.

The pump 1 diode, similar to the seed diode, features a narrow linewidth, but also experiences linewidth broadening and wavelength drift with scaling output power and operating temperature, as characterized previously in Section 3.3. The pump 1 diode features a 0.81 W/A slope efficiency and was initially characterized up to 9 A drive current due to thermal related limitations in the initial laser construction, however, during the characterization of the first and second amplification stages, the diode is driven up to 11 A. The expected output power has been interpolated for drive currents of 9.5, 10, 10.5, and 11 A respectively. At the chosen maximum output power, 11 A for $P_{Out} = 9.190$ W, and given the trendline for the center wavelength and full width at half maximum measurements, we expect a $\lambda_{FWHM} = 0.24$ nm and a $\lambda_c = 976.0$ nm.

4.1.3 Pump 2 Diode

The laser diode utilized to pump the second amplification stage is the Element-06 n-Light diode. This laser diode emits a continuous wave multimode beam centered at $\lambda_c = 976\pm1$ nm, and λ_{FWHM} ranging between 0.3-1 nm, up to a maximum output power of 60 W, at 14 A drive current, according to the manufacturer specifications. The diode has a standard operating temperature of 30°C. The diode also comes prepackaged with a diode-fiber combiner to a NA = 0.22 multimode 105/125 μm fiber. The in-lab characterization details are provided in Figure 29.
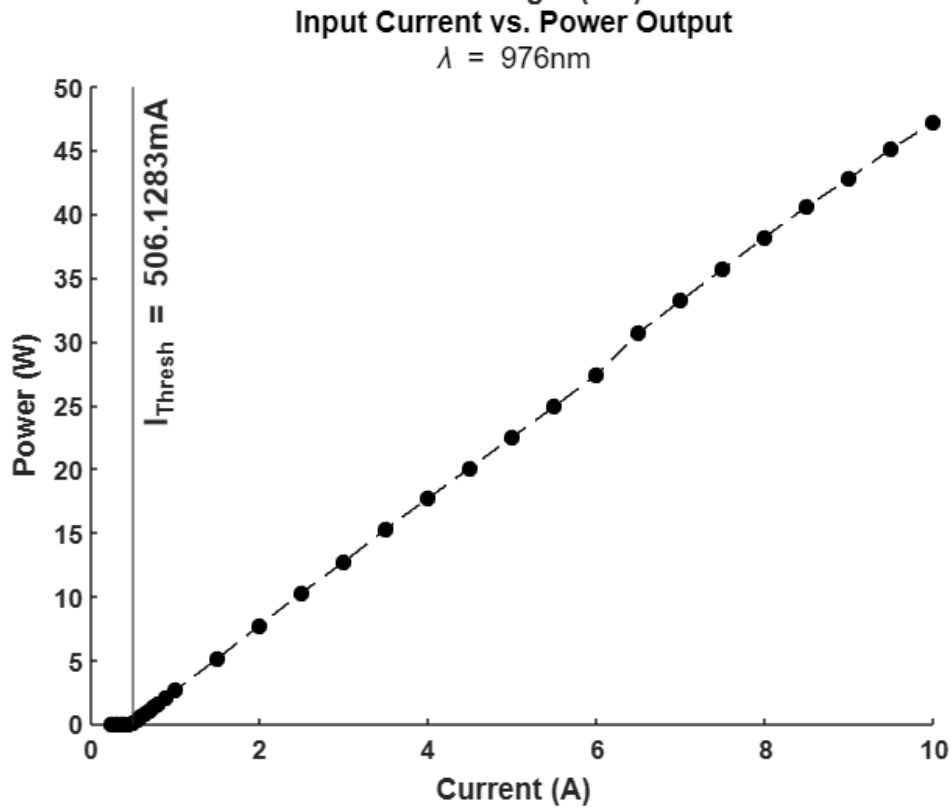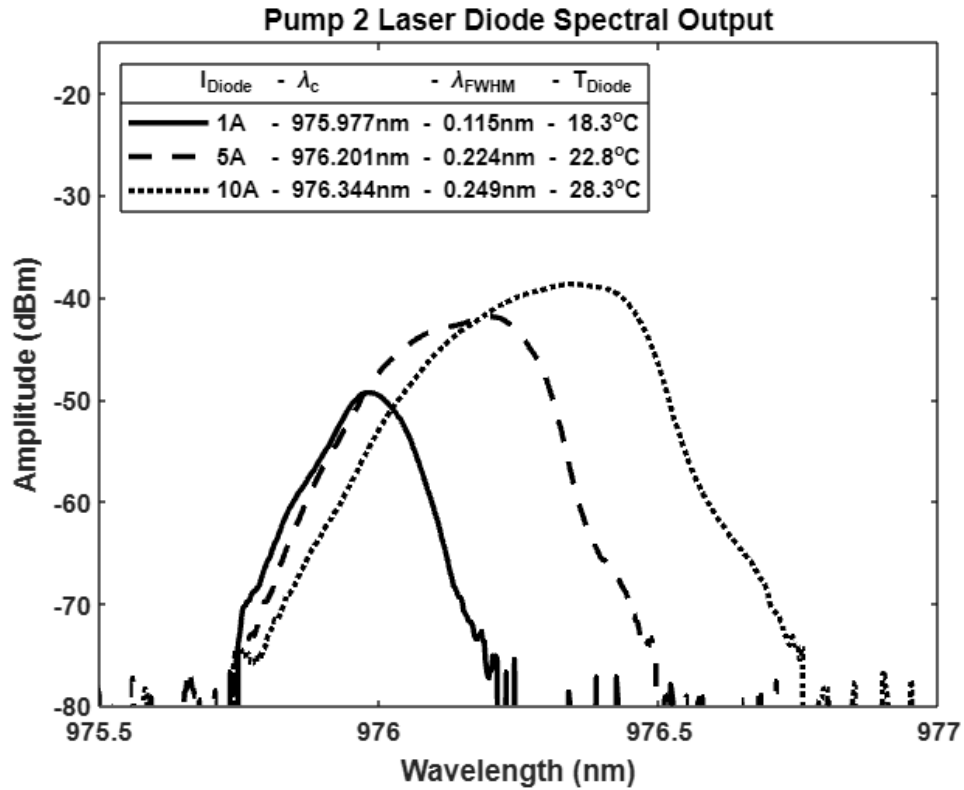
Figure 29: Pump 2 laser diode characterizations. [Top] Pump 2 spectral data. [Bottom] Pump 2

P-I curve.

The pump 2 diode also features a narrow linewidth and experiences linewidth broadening and wavelength drift with scaling output power and operating temperature. The pump 2 diode features a tremendous 5.02 W/A slope efficiency and an I_{Thresh} = 506 mA. Although characterized here up to 9 A drive current for 42.8 W of output power the pump 2 diode was not driven past 4 A (17.7 W) so that the max input power of the following passive fiber components would not be exceeded. Further information on the operating specifications of the passive components utilized in the construction of the Yb-doped MOPA fiber laser can be referenced in Table 1. At the chosen maximum output power to be utilized, 4.8 A for P_{Out} = 21.54 W, we expect a λ_{FWHM} = 0.18 nm and a λ_c = 975.73 nm.

There are slight variations between the manufacturer and in-lab characterizations, which are most likely due to the inability to meet the exact operating conditions utilized by the manufacturer. Nevertheless, the diode characteristics measured are capable of satisfying the signal and pumping needs of the Yb-doped MOPA fiber laser system being developed.

4.2 First Amplification Stage Characterization

This section provides an outlook on the active fiber pumping and signal characteristics. The optical power injected into the first amplification fiber originate within the seed and pump 1 diodes, both of which were characterized in section 4.1, however, both the signal and pump power pass through multiple passive fiber components with known insertion losses. As a result, the input powers into the first amplification stage that are referenced are characterized at the first combiner output before the splicing of the first active fiber.

Since the seed current is always run at maximum output power, it was characterized at 800 mA of injection current. It yielded a signal power output of 348 mW, down from the 366 mW measured

directly out of the seed diode coupled fiber. This indicates a 0.22 dB difference, which is ideal, considering the maximum insertion loss for the first isolator (1 dB) and pump combiner (0.5 dB) and the accompanying splices that the signal traverses. The expected and measured losses for both the signal and pump power and their expected sources are included in Table 3. The measured losses being beneath the expected losses support the assumption that the devices are operating normally and that the accompanying splices are satisfactory. With this data, an accurate characterization of the first amplification fiber can be made.

Table 3: Passive fiber component insertion losses vs. the actual losses leading into the first amplification fiber.

	Traversed Passive Components	Max Insertion Loss (dB)	Input Power (W)	Output Power (W)	Measured Losses (dB)
Seed (800mA)	Isolator 1 + Pump Combiner 1	1 + 0.5	0.366	0.348	0.22
Pump 1 (11A)	Pump Combiner 1	0.5	9.19	8.18	0.51

Approximately 2.5 m of PLMA-YDF-10/125-HI-8 double clad optical fiber is utilized in the first amplification stage. 348 mW of 1064 nm signal power is injected into the fiber and the 976 nm pump power, originating from the pump 1 diode, was varied. Figure 30 depicts the obtained broadband spectral data and conversion efficiencies from the resulting amplification, measured out of the approximately 4° angle cleaved active fiber end directed into the beam sampling optical setup described in Section 3.4.
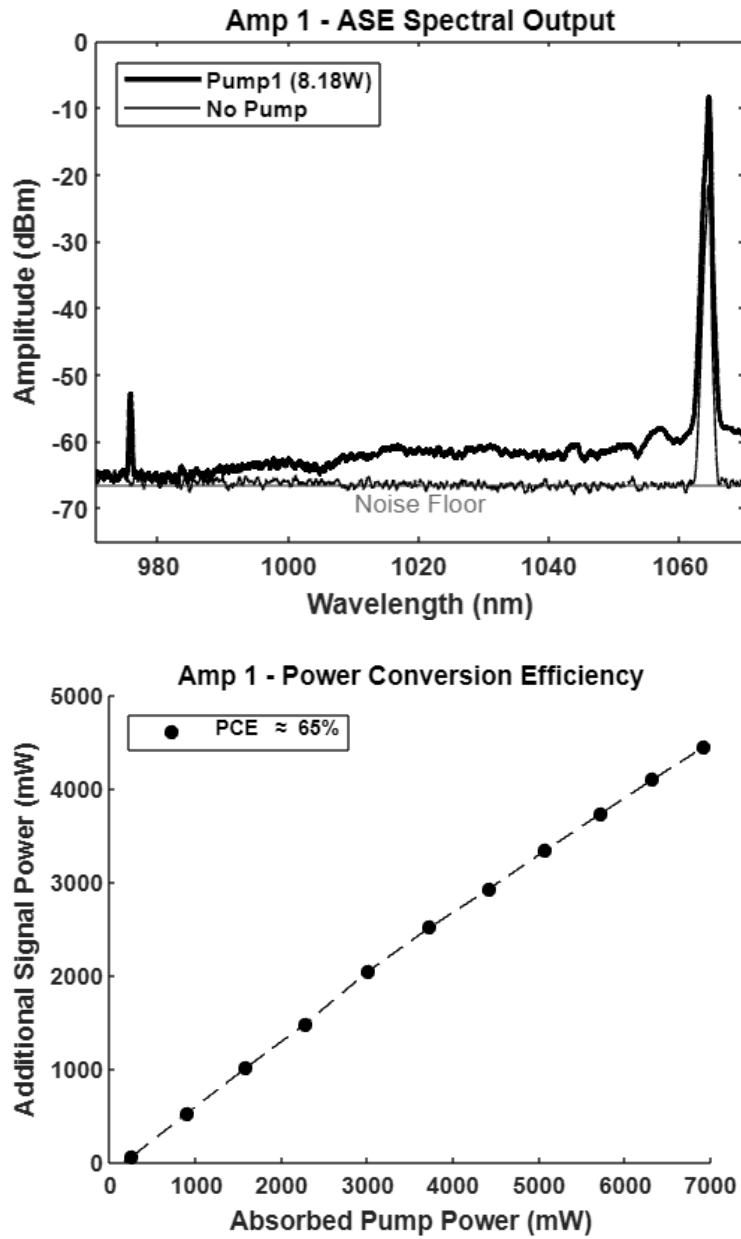
Figure 30: Stage 1 amplification characterizations. [Top] 970-1070 nm spectral data and [Bottom] conversion efficiency of 2.5 m Yb-doped active fiber averaging near 65%.

The spectral output includes the optical emissions before and after activating the pump 1 diode. Before pump activation, only the signal spectrum is captured and the noise floor of the OSA is observed at -66.5 dBm. Upon activating the pump 1 diode, a spike at 976 nm appears, due to unabsorbed pump light exiting the active fiber and the noise floor is raised in the 970-1100 nm

range due to ASE. This range lines up with the broader expected gain spectra for Yb-doped fiber, provided in Figure 4. No evidence of parasitic lasing is observed. Unabsorbed pump power is not ideal; however, the maximum observed ASE levels are measured approximately 50 dB below the signal peak and sufficient pump conversion has been achieved. This signal-to-noise ratio is well above the levels at which ASE becomes a threatening condition in latter amplification stages.

The total optical powers exiting the 2.5 m of active fiber are as follows: 4.83 W of signal and 1.34 W of pump. Therefore, the measured conversion efficiencies lie near 65% as 348 mW and 8.27 W of injected signal and pump power results in 6.93 W of absorbed pump power being converted to 4.48 W of additional signal power. It is expected that a longer length of fiber would result in additional absorption of the pump power, and a resulting increase in the conversion efficiency of this amplification stage. However, increasing the fiber length too much may result in an increased ASE to signal ratio as the signal is reabsorbed in under-pumped lengths of active fiber. Because the current ASE levels are low, and the resultant emitted signal power is satisfactory, the design of the first amplification stage is considered satisfactory for signal generation into the next stage of the Yb-doped MOPA fiber laser.

4.3 Second Amplification Stage & Final Characterization

In the characterization of the second amplification stage, the signal output of the first amplification fiber acts as the signal input of the second amplification fiber, with the intermediate losses from passive fiber components being considered. The excess pump light exiting the first active fiber is dumped on the transition through isolator 2 since the pump light lies outside the operating wavelength of that component. The measured losses through each passive fiber component is recorded in Table 4.

Table 4: Passive fiber component insertion losses vs. the actual losses leading into the second amplification fiber.

	Traversed Passive Components	Max Insertion Loss (dB)	Input Power (W)	Output Power (W)	Measured Losses (dB)
Signal	Isolator 2 + Pump Combiner 2	1 + 0.5	4.83	4.68	0.14
Residual Pump	Isolator 2	-	1.34	~0	>40
Pump 2 (4.8A)	Pump Combiner 2	0.5	21.54	20	0.32

The measured insertion losses lie below the maximum losses for the individual passive fiber components, indicating satisfactory optical coupling. Approximately 4.5 m of Yb-doped fiber is used in the second amplification stage. 4.68 W of 1064 nm signal power is injected into the fiber, originating from the first amplification stage, and the 976 nm pump input power is independently varied, originating from the pump 2 diode. Figure 31 depicts the broadband spectral data and conversion efficiencies from the resulting amplification, measured using previous methods.
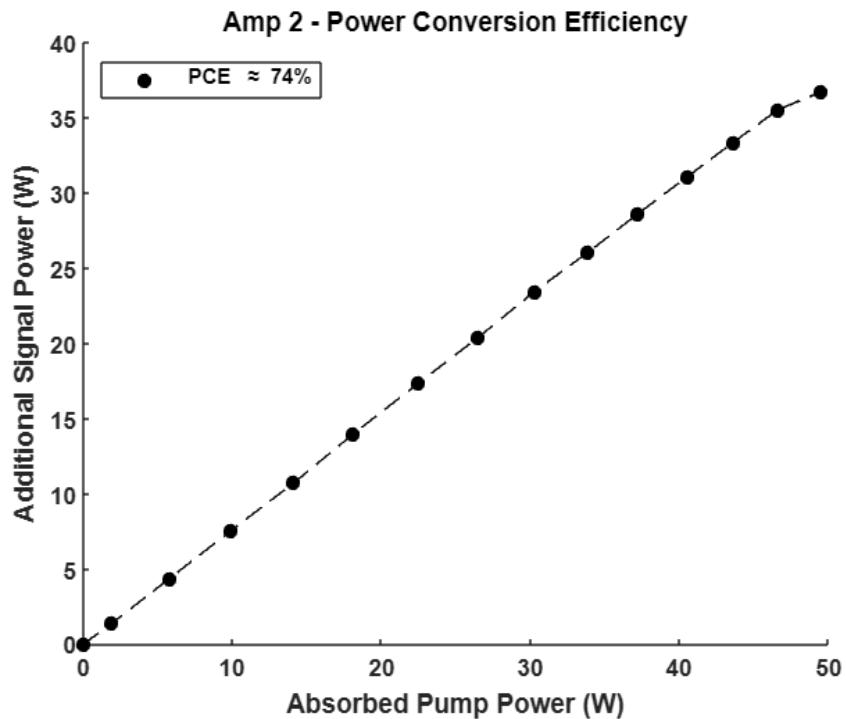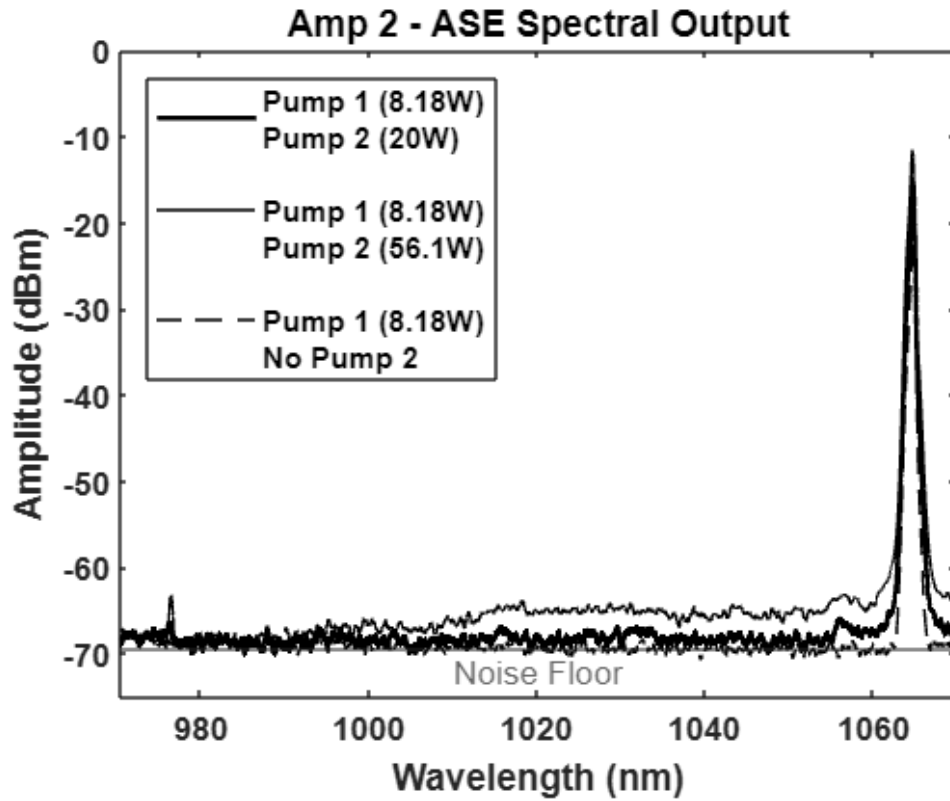
Figure 31: Stage 2 amplification characterizations. [Top] 970-1070 nm spectral data and

[Bottom] conversion efficiency of 4.5 m Yb-doped active fiber.

In Figure 31, the second pump diode is driven past the expected output power threshold of the system. This is possible because the output is being sampled out of the second Yb-doped fiber, therefore, the input power restrictions of the following passive fiber components are not yet applicable. In terms of ASE generation, even at pump 2 injection powers significantly higher (56.1 W) than what is needed (20 W) to meet the final system specifications, there is still an approximate 51 dB difference between the ASE and signal peak amplitudes. Also observed, is a noticeably higher conversion efficiency through the longer 4.5 m active fiber.

The total optical powers exiting the 4.5 m of active fiber are as follows: 17.7 W of signal and 2.75 W of pump. The calculated conversion efficiencies lie near 75% for the second amplifier as 4.68 W and 20 W of injected signal and pump power results in 17.25 W of absorbed pump power being converted to 13.02 W of additional signal power. After splicing on the in-lab made cladding light stripper and circulator, the final laser characterizations are performed. Table 5 lists the expected and measured losses from the final passive fiber components.

Table 5: Final passive fiber component expected insertion losses vs. the actual measured losses.

	Traversed Passive Components	Max Insertion Loss (dB)	Input Power (W)	Output Power (W)	Measured Losses (dB)
Seed	Cladding Light Stripper + Circulator	0 + 0.78	17.7	16.4	0.33
Residual Pump	Cladding Light Stripper	-	2.67	0	>40

With these passive components spliced onto the system, the limiting factor for output power becomes the maximum input power of the circulator, which is 20 W. All following characterizations of the laser output power and spectral output become capped at 16.4 W of total signal output power as a result due to the insertion loss experienced at the circulator. This maximum output power is achieved with the following input parameter specifications:

The seed laser diode is driven at 800 mA for 366 mW signal power generation, resulting in 348 mW injection into the first 2.5 m amplifying fiber. The first pump laser diode is driven at 11 A for 9.19 W pump power generation, resulting in 8.18 W injection into the first 2.5 m amplifying fiber. The subsequent amplification in the 2.5 m fiber results in 4.83 W of signal and 1.34 W of excess pump emissions out of the end of the first active fiber, yielding a conversion efficiency of 65%. Of that, 4.68 W of signal power is injected into the second 4.5 m amplifying fiber. The second pump laser diode is driven at 4.8 A for approximately 21.54 W of pump power generation, resulting in approximately 20 W injection into the second 4.5 m amplifying fiber. The subsequent amplification in the 4.5 m fiber results in approximately 17.7 W of signal and 2.67 W of excess pump emissions out of the end of the second active fiber, yielding a conversion efficiency of 75%. Of that, 16.4 W of signal power is emitted out of the Yb-doped MOPA fiber laser system. The pump power is stripped from the final emission. The final laser characterization is obtained when running with these specific operating conditions. The final laser spectral data and P-I curve is provided in Figure 32.
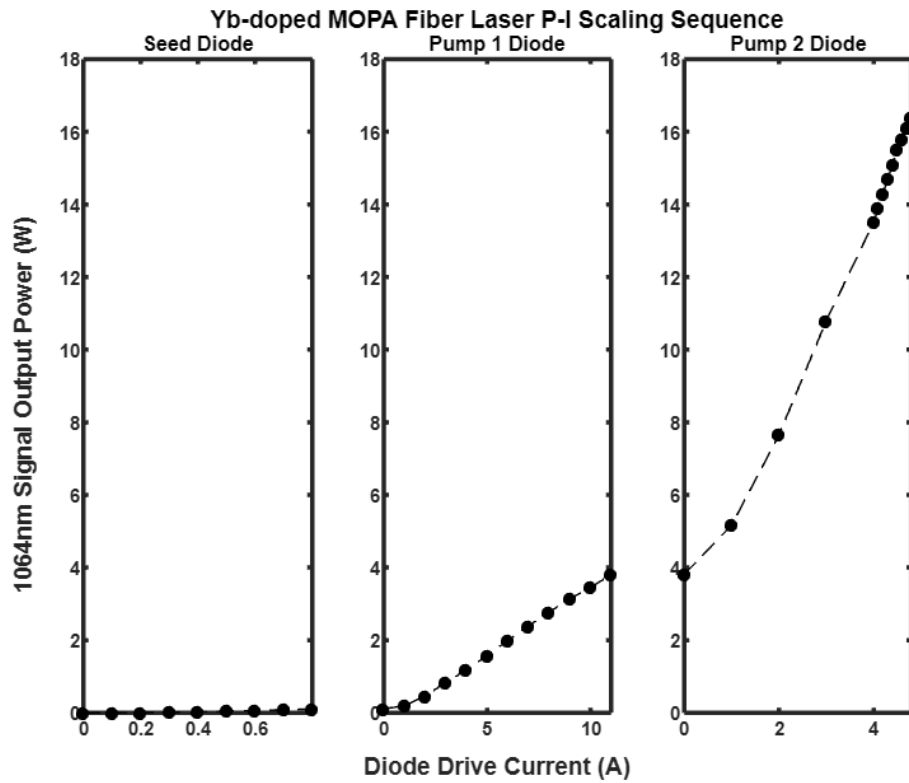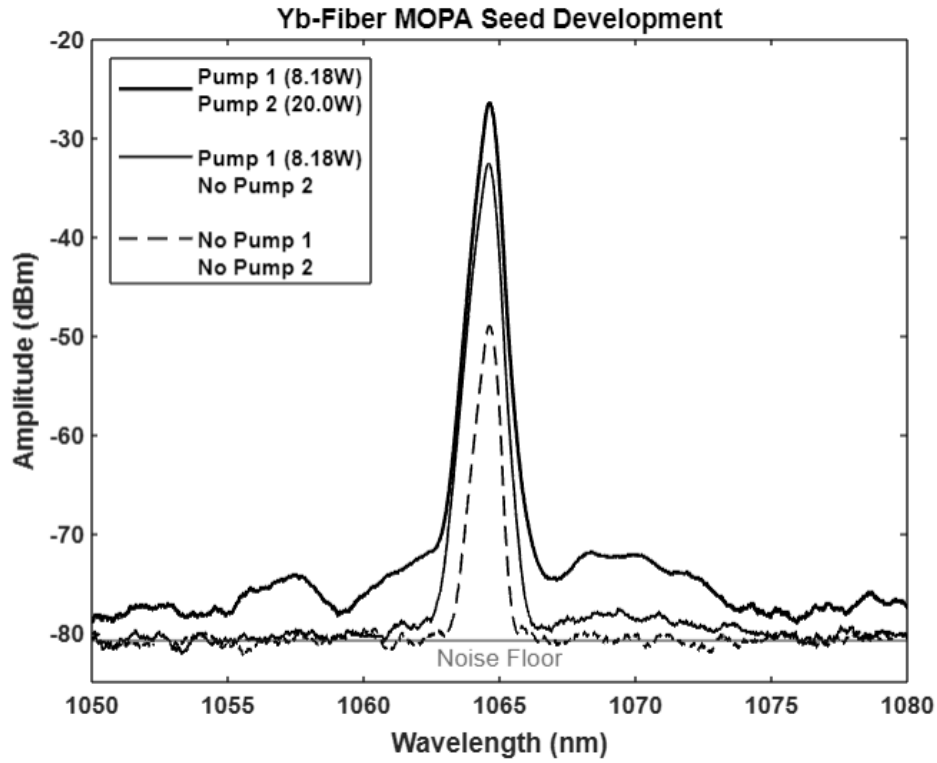
Figure 32: Final Yb-doped MOPA laser system characterizations. [Top] 1050-1080 nm spectral

data at various operating regimes and [Bottom] signal output power vs. diode current.

This fiber laser system emits a high-quality CW single mode beam that is polarized along the slow axis of the emitting PM optical fiber. The initial signal output power is scaled from 366 mW to 16.4 W while maintaining a λ_c = 1064.8nm and a λ_{FWHM} of 0.21 nm. A 46 dB difference between the signal and ASE peak is observed with no evidence of internal parasitic lasing. and a total optical conversion efficiency of approximately 72% are maintained within the active fiber. This efficiency calculation accounts for the total signal power generated (17.7 W) minus the injected signal power (348 mW) divided by the total injected pump power that was absorbed (24.17 W). This optical conversion efficiency is in line with other 1 µm CW Yb-doped fiber amplifiers pumped at 976 nm optical conversion efficiencies ranging between 65% and 90%, [13, 16, 59-61]. Accounting for system internal losses, i.e., wasted pump power and passive component insertion losses, a system optical efficiency of 52% is calculated, as 16.4 W minus 0.366 mW of signal power is produced from 9.19 W and 21.54 W of pump power from pump 1 and 2, respectively. The system electro-optical efficiency is 27%. A final system amplification factor of A_F = 44.81 = 366mW/16.4W is achieved.

The optical conversion efficiency of this system could be improved with increased fiber lengths for both amplifying stages, as there was significant unabsorbed pump power measured at their outputs (1.34 W and 2.67 W for amplification stages 1 and 2). However, this would have come at the cost of increased ASE-signal levels. It was determined to prioritize signal quality over conversion efficiency as the output of this system is intended to act as a seeding device for a following high power amplification stage.

CHAPTER 5: CONCLUSIONS

The constructed Yb-doped MOPA fiber laser system has been successfully constructed. All of the specifications required for integration into the following Yb-doped fixed wavelength kilowatt fiber laser system for the expected thermal blooming experiments have been met. Although the primary objective of the laser's construction has been achieved, secured operation of the system requires a certain degree of understanding in the underlying photonics at play within the laser system's design.

The most notable operating characteristic of the Yb-doped MOPA fiber laser, to be considered, is the booting up procedure. MOPA fiber lasers feature incredible risk in the powering on procedure as the long lengths of active fiber can lead to the excessive amplification of unwanted frequencies, modes, or pulses traversing the fiber components which become much more chaotic when strong ASE is prevalent. The amplification potential for these instabilities can lead to the generation of intra-fiber intensities that can damage the coupled fiber components or the fibers themselves.

This particular laser system was a victim of such risk. As the pump diodes were operating near maximum pump power, the seed current was digitally altered by the operator. The change resulted in the seed diode powering off before re-lasing at the designated output power. The brief moment where the seed shutdown resulted in one of the active fibers to fracture and the permanent damaging of the seed diode. Additional damage could also take place within the MOPA fiber laser as the pumps were still actively pumping the active fiber for several seconds before an emergency shutoff was activated. It is hypothesized that in this time, a frequency channel contributing to ASE developed a resonant channel within the fiber laser system and was systematically amplified as it successfully competed for gain within the active fibers. Such a case can lead to the generation of

extremely high power picosecond optical pulses that far exceed the maximum operating conditions of the fiber components.

It was noted, in the construction of the laser system, how crucial it was to log transmitted powers through every intermediate component or splice performed in its construction. As multiple layers are added to the holistic system, the operating limitations of every subsequent device would stack and would need to be considered when operating the laser. For example, although the pump 2 diode could successfully pump the second amplification stage at its maximum operating power with minimal ASE generation, it became crucial not to power it over 20 W as the maximum insertion load of the following cladding light stripper and circulator would need to be adhered to.

In addition to the powering on sequence, it is critical that the laser diodes, active fiber, and coupled fiber components are actively cooled during operation of the laser system. As detailed in Section 3.3, the diodes can heat significantly past their specified operating temperatures if no active cooling mechanisms are implemented. The overheating of the semiconductor diodes can lead to diode failure or extreme wavelength drift contributing towards disorder of the internal amplification process.

Similar to the development of the thermal management approaches, there was a significant degree of trial and error experienced in the initial stages of the laser's development provided towards the fiber processing techniques utilized in the construction of this system. Approaches taken for fiber preparation for splicing and the methods used to check their quality thereafter were continuously modified to produce techniques with greater success rates. Although this system features only 10 splices, more than double this amount resulted in failed splices. In the surviving splices, various polymers and splice recipes were used to ensure proper throughput between the fibers.

These considerations when building and operating a fiber laser system shows the need for a large underlying base of knowledge on the innerworkings and risks associated with their development, and more particularly, the development of MOPA fiber laser systems.

REFERENCES

[1]   (2023). *GAO-23-105868, DIRECTED ENERGY WEAPONS DOD Should Focus on Transition Planning*. [Online] Available: https://www.gao.gov/assets/gao-23-105868.pdf

[2]   F. G. Gebhardt and D. C. Smith, "Effects of Wind on Thermal Defocusing of CO2 Laser Radiation," *Applied Physics Letters,* vol. 14, no. 2, pp. 52-54, 1969, doi: 10.1063/1.1652708.

[3]   P. V. Avizonis, C. B. Hogge, R. R. Butts, and J. R. Kenemuth, "Geometric Optics of Thermal Blooming in Gases. Part 1," *Appl. Opt.,* vol. 11, no. 3, pp. 554-564, 1972/03/01 1972, doi: 10.1364/AO.11.000554.

[4]   M. F. Spencer, "Branch Point Mitigation of Thermal Blooming Phase Compensation Instability," 2012.

[5]   T. H. Maiman, "Stimulated Optical Radiation in Ruby," *Nature,* vol. 187, no. 4736, pp. 493-494, 1960/08/01 1960, doi: 10.1038/187493a0.

[6]   A. L. Schawlow and C. H. Townes, "Infrared and Optical Masers," *Physical Review,* vol. 112, no. 6, pp. 1940-1949, 12/15/ 1958, doi: 10.1103/PhysRev.112.1940.

[7]   E. Snitzer, "Optical Maser Action of Nd^{+3} in a Barium Crown Glass," *Physical Review Letters,* vol. 7, no. 12, pp. 444-446, 12/15/ 1961, doi: 10.1103/PhysRevLett.7.444.

[8]   H. Po *et al.*, "DOUBLE CLAD HIGH BRIGHTNESS Nd FIBER LASER PUMPED BY GaAlAs PHASED ARRAY," in *Optical Fiber Communication Conference*, Houston, Texas, 1989/02/06 1989, vol. 5: Optica Publishing Group, in 1989 OSA Technical Digest Series, p. PD7, doi: 10.1364/OFC.1989.PD7. [Online]. Available: https://opg.optica.org/abstract.cfm?URI=OFC-1989-PD7

[9]   W. A. Clarkson, N. Barnes, P. W. Turner, J. Nilsson, and D. Hanna, "High-power cladding-pumped Tm-doped silica fiber laser with wavelength tuning from 1860 to 2090 nm," *Opt. Lett.,* vol. 27, pp. 1989-91, 11/01 2002, doi: 10.1364/OL.27.001989.

[10]   E. Snitzer, "Cylindrical Dielectric Waveguide Modes*," *J. Opt. Soc. Am.,* vol. 51, no. 5, pp. 491-498, 1961/05/01 1961, doi: 10.1364/JOSA.51.000491.

[11]   A. Tünnermann *et al.*, "The renaissance and bright future of fibre lasers," *Journal of Physics B: Atomic, Molecular and Optical Physics,* vol. 38, no. 9, p. S681, 2005/04/25 2005, doi: 10.1088/0953-4075/38/9/016.

[12]   D. J. Richardson, J. Nilsson, and W. A. Clarkson, "High Power Fiber Lasers: Current Status and Future Perspectives," *JOSA B,* vol. 27, pp. B63-B92, 11/01 2010, doi: 10.1364/JOSAB.27.000B63.

[13] Y. Jeong *et al.*, "Power Scaling of Single-Frequency Ytterbium-Doped Fiber Master-Oscillator Power-Amplifier Sources up to 500 W," *IEEE Journal of Selected Topics in Quantum Electronics,* vol. 13, no. 3, pp. 546-551, 2007, doi: 10.1109/JSTQE.2007.896639.

[14] J. Cook, "High Power Ytterbium and Thulium Fiber Lasers," Doctor of Philosophy (Ph.D.), Optics and Photonics, University of Central Florida, STARS UCF, 2021. [Online]. Available: https://purls.library.ucf.edu/go/DP0026091

[15] Y. Jeong, J. K. Sahu, D. N. Payne, and J. Nilsson, "Ytterbium-doped large-core fiber laser with 1.36 kW continuous-wave output power," *Opt. Express,* vol. 12, no. 25, pp. 6088-6092, 2004/12/13 2004, doi: 10.1364/OPEX.12.006088.

[16] A. Liem *et al.*, "1.3 kW Yb-doped fiber laser with excellent beam quality," in *Conference on Lasers and Electro-Optics/International Quantum Electronics Conference and Photonic Applications Systems Technologies*, San Francisco, California, 2004/05/16 2004: Optica Publishing Group, in Technical Digest (CD), p. CPDD2. [Online]. Available: https://opg.optica.org/abstract.cfm?URI=CLEO-2004-CPDD2. [Online]. Available: https://opg.optica.org/abstract.cfm?URI=CLEO-2004-CPDD2

[17] G. P. Agrawal, "Nonlinear Fiber Optics," in *Nonlinear Science at the Dawn of the 21st Century*, Berlin, Heidelberg, P. L. Christiansen, M. P. Sørensen, and A. C. Scott, Eds., 2000// 2000: Springer Berlin Heidelberg, pp. 195-211.

[18] G. P. Agrawal, *Nonlinear Fiber Optics*. Elsevier Inc., 2019.

[19] S. J. Augst, A. K. Goyal, R. L. Aggarwal, T. Y. Fan, and A. Sanchez, "Wavelength beam combining of ytterbium fiber lasers," *Opt. Lett.,* vol. 28, no. 5, pp. 331-333, 2003/03/01 2003, doi: 10.1364/OL.28.000331.

[20] M. Karow, J. Neumann, D. Kracht, and P. Weßels, "Impact of amplified spontaneous emission on Brillouin scattering of a single-frequency signal," *Opt. Express,* vol. 20, no. 10, pp. 10572-10582, 2012/05/07 2012, doi: 10.1364/OE.20.010572.

[21] O. G. Okhotnikov, L. Gomes, N. Xiang, T. Jouhti, and A. B. Grudinin, "Mode-locked ytterbium fiber laser tunable in the 980–1070-nm spectral range," *Opt. Lett.,* vol. 28, no. 17, pp. 1522-1524, 2003/09/01 2003, doi: 10.1364/OL.28.001522.

[22] T. Newell, P. Peterson, A. Gavrielides, and M. P. Sharma, "Temperature Effects on the Emission Properties of Yb-Doped Fiber (Postprint)," p. 9, 11/29 2006.

[23] V. V. Ter-Mikirtychev, *Fundamentals of Fiber Lasers and Fiber Amplifiers*, 2 ed. (Springer Series in Optical Sciences). Springer Cham, 2019, p. 330.

[24] M. Ilchi-Ghazaani and P. Parvin, "Gain Saturation in Optical Fiber Laser Amplifiers," 2016, pp. 297-320.

[25]   S. Unger *et al.*, "A highly efficient Yb-doped silica laser fiber prepared by gas phase doping technology," *Laser Physics,* vol. 24, 02/11 2014, doi: 10.1088/1054-660X/24/3/035103.

[26]   *4.3 Diode-pumped fiber lasers: Datasheet from Landolt-Börnstein - Group VIII Advanced Materials and Technologies · Volume 1B2: "Laser Systems, Part 2" in SpringerMaterials (https://doi.org/10.1007/978-3-540-45867-8_3).* Springer-Verlag Berlin Heidelberg. [Online]. Available: https://materials.springer.com/lb/docs/sm_lbs_978-3-540-45867-8_3

[27]   R. Paschotta, J. Nilsson, A. C. Tropper, and D. C. Hanna, "Ytterbium-doped fiber amplifiers," *IEEE Journal of Quantum Electronics,* vol. 33, no. 7, pp. 1049-1056, 1997, doi: 10.1109/3.594865.

[28]   J. A.-O. Mirza *et al.*, "Performance Enhancement of Ytterbium-Doped Fiber Amplifier Employing a Dual-Stage In-Band Asymmetrical Pumping. LID - 10.3390/mi13091488 [doi] LID - 1488," (in eng), no. 2072-666X (Print).

[29]   F. He, J. H. V. Price, K. T. Vu, A. Malinowski, J. K. Sahu, and D. J. Richardson, "Optimisation of cascaded Yb fiber amplifier chains using numerical-modelling," *Opt. Express,* vol. 14, no. 26, pp. 12846-12858, 2006/12/25 2006, doi: 10.1364/OE.14.012846.

[30]   T. Taira, W. M. Tulloch, and R. L. Byer, "Modeling of quasi-three-level lasers and operation of cw Yb:YAG lasers," *Appl. Opt.,* vol. 36, no. 9, pp. 1867-1874, 1997/03/20 1997, doi: 10.1364/AO.36.001867.

[31]   A. El Sayed, S. Pilz, H. Najafi, D. T. L. Alexander, M. Hochstrasser, and V. Romano, "Fabrication and Characteristics of Yb-Doped Silica Fibers Produced by the Sol-Gel Based Granulated Silica Method," *Fibers*, vol. 6, no. 4*,* doi: 10.3390/fib6040082.

[32]   K. V. Krishnaiah *et al.*, "Fluorescence and Spectroscopic Properties of Yb3+-Doped Phosphate Glasses," *Physics Procedia,* vol. 29, pp. 109-113, 2012/01/01/ 2012, doi: https://doi.org/10.1016/j.phpro.2012.03.700.

[33]   G. E. Peterson and P. M. Bridenbaugh, "Study of Relaxation Processes in Nd Using Pulsed Excitation," *J. Opt. Soc. Am.,* vol. 54, no. 5, pp. 644-650, 1964/05/01 1964, doi: 10.1364/JOSA.54.000644.

[34]   B. Wilhelm, V. Romano, and H. P. Weber, "Fluorescence lifetime enhancement of Nd3+-doped sol–gel glasses by Al-codoping and CO2-laser processing," *Journal of Non-Crystalline Solids,* vol. 328, no. 1, pp. 192-198, 2003/10/15/ 2003, doi: https://doi.org/10.1016/S0022-3093(03)00366-1.

[35]   J. E. Geusic, H. M. Marcos, and L. G. Van Uitert, "LASER OSCILLATIONS IN Nd-DOPED YTTRIUM ALUMINUM, YTTRIUM GALLIUM AND GADOLINIUM GARNETS," *Applied Physics Letters,* vol. 4, no. 10, pp. 182-184, 2004, doi: 10.1063/1.1753928.

[36]   K. F. Renk, *Basics of Laser Physics* (Graduate Texts in Physics). Springer Cham, 2012, pp. XIX, 676.

[37]   W. F. Krupke, "Ytterbium solid-state lasers. The first decade," *IEEE Journal of Selected Topics in Quantum Electronics,* vol. 6, no. 6, pp. 1287-1296, 2000, doi: 10.1109/2944.902180.

[38]   *RP Fiber Power [Computer Software].* (2020). RP Photonics Consulting GmbH.

[39]   P. Parvin, M. Ilchi-Ghazaani, A. Bananej, and Z. Lali-Dastjerdi, "Small signal gain and saturation intensity of a Yb:Silica fiber MOPA system," *Optics & Laser Technology,* vol. 41, no. 7, pp. 885-891, 2009/10/01/ 2009, doi: https://doi.org/10.1016/j.optlastec.2009.02.006.

[40]   P. L. Friedrich Bachman, Reinhart Poprawe, *High Power Diode Lasers*, 1 ed. (Springer Series in Optical Sciences). 2007, pp. VI, 554.

[41]   T. Numai, *Fundamentals of Semiconductor Lasers* (Springer Series in Optical Sciences). 2004, pp. XII, 268.

[42]   N. B. Abraham, L. A. Lugiato, and L. M. Narducci, "Overview of instabilities in laser systems," *J. Opt. Soc. Am. B,* vol. 2, no. 1, pp. 7-14, 1985/01/01 1985, doi: 10.1364/JOSAB.2.000007.

[43]   C. O. Weiss, "Chaotic laser dynamics," *Optical and Quantum Electronics,* vol. 20, no. 1, pp. 1-22, 1988/01/01 1988, doi: 10.1007/BF02069690.

[44]   L. Chen, R. Song, C. Lei, W. Yang, F. He, and J. Hou, "Influences of position of ytterbium-doped fiber and ASE pump on spectral properties of random fiber laser," *Opt. Express,* vol. 27, no. 7, pp. 9647-9654, 2019/04/01 2019, doi: 10.1364/OE.27.009647.

[45]   O. Svelto, *Principles of Lasers*. Springer New York, NY, 2010, pp. XXI, 620.

[46]   G. Canat *et al.*, "Power limitations of fiber lasers at 1.5 µm by parasitic lasing effects," in *Conference on Lasers and Electro-Optics/International Quantum Electronics Conference and Photonic Applications Systems Technologies*, San Francisco, California, 2004/05/16 2004: Optica Publishing Group, in Technical Digest (CD), p. CMK6. [Online]. Available: https://opg.optica.org/abstract.cfm?URI=CLEO-2004-CMK6. [Online]. Available: https://opg.optica.org/abstract.cfm?URI=CLEO-2004-CMK6

[47]   Z. Li, S. Zhou, A. Liu, J. Cao, Z. Huang, and J. Chen, "Experimental Study on the In-Band Amplified Spontaneous Emission in the Single-Mode Continuous-Wave Yb-Doped Fiber Amplifier Operating near 980 nm," *Photonics*, vol. 9, no. 6, doi: 10.3390/photonics9060377.

[48]   P.-Y. Lai, C.-L. Chang, S.-L. Huang, and S.-H. Chen, "Influences of Amplified Spontaneous Emission on Fiber Laser Amplifier Chain," in *2013 Conference on Lasers and Electro-Optics Pacific Rim*, Kyoto, 2013/06/30 2013: Optica Publishing Group, p.

WPA_29. [Online]. Available: https://opg.optica.org/abstract.cfm?URI=CLEOPR-2013-WPA_29. [Online]. Available: https://opg.optica.org/abstract.cfm?URI=CLEOPR-2013-WPA_29

[49]   A. Silva, K. J. Boller, and I. D. Lindsay, "Wavelength-swept Yb-fiber master-oscillator-power-amplifier with 70nm rapid tuning range," *Opt. Express,* vol. 19, no. 11, pp. 10511-10517, 2011/05/23 2011, doi: 10.1364/OE.19.010511.

[50]   Brahma N. Upadhyaya, A. Kuruvilla, U. Chakravarty, Mangalpady R. Shenoy, K. Thyagarajan, and Shrikant M. Oak, "Effect of laser linewidth and fiber length on self-pulsing dynamics and output stabilization of single-mode Yb-doped double-clad fiber laser," *Appl. Opt.,* vol. 49, no. 12, pp. 2316-2325, 2010/04/20 2010, doi: 10.1364/AO.49.002316.

[51]   S. Wang, X. Lin, Z. Zhang, Y. Xing, L. Liao, and J. Li, "All-fiber pulsed laser generation of 25.5 mJ and solution of parasitic oscillation," *Appl. Opt.,* vol. 60, no. 5, pp. 1117-1120, 2021/02/10 2021, doi: 10.1364/AO.409564.

[52]   R. Paschotta, *Field Guide to Optical Fiber Technology* (SPIE Field Guides). SPIE, 2010.

[53]   A. R. Tynes, A. D. Pearson, and D. L. Bisbee, "Loss Mechanisms and Measurements in Clad Glass Fibers and Bulk Glass," *J. Opt. Soc. Am.,* vol. 61, no. 2, pp. 143-153, 1971/02/01 1971, doi: 10.1364/JOSA.61.000143.

[54]   (2021). *A Brief Introduction to Core Modes in Optical Fiber*. [Online] Available: https://apps.dtic.mil/sti/pdfs/AD1124366.pdf

[55]   A. D. Yablon, *Optical Fiber Fusion Splicing* (Springer Series in Optical Sciences). 2005.

[56]   R. Janani *et al.*, "From acrylates to silicones: A review of common optical fibre coatings used for normal to harsh environments," *Progress in Organic Coatings,* vol. 180, p. 107557, 2023/07/01/ 2023, doi: https://doi.org/10.1016/j.porgcoat.2023.107557.

[57]   D. Gloge, P. W. Smith, D. L. Bisbee, and E. L. Chinnock, "Optical fiber end preparation for low-loss splices," *The Bell System Technical Journal,* vol. 52, no. 9, pp. 1579-1588, 1973, doi: 10.1002/j.1538-7305.1973.tb02034.x.

[58]   C. A. Millar and D. J. Gooch, "Optimizing cleaving tools by end-angle measurement," in *Optical Fiber Communication*, New Orleans, Louisiana, 1983/02/28 1983: Optica Publishing Group, in OSA Technical Digest, p. MG2, doi: 10.1364/OFC.1983.MG2. [Online]. Available: https://opg.optica.org/abstract.cfm?URI=OFC-1983-MG2

[59]   Y. Jeong, J. K. Sahu, D. N. Payne, and J. Nilsson, "Ytterbium-doped large-core fibre laser with 1 kW of continuous-wave output power," *Electronics Letters*, vol. 40, no. 8, pp. 470-472. [Online]. Available: https://digital-library.theiet.org/content/journals/10.1049/el_20040298

[60]   Y. Jeong *et al.*, "Single-frequency, single-mode, plane-polarized ytterbium-doped fiber master oscillator power amplifier source With 264 W of output power," *Opt. Lett.,* vol. 30, pp. 459-61, 04/01 2005, doi: 10.1364/OL.30.000459.

[61]   S. Höfer *et al.*, "Single-frequency master-oscillator fiber power amplifier system emitting 20 W of power," *Opt. Lett.,* vol. 26, no. 17, pp. 1326-1328, 2001/09/01 2001, doi: 10.1364/OL.26.001326.